

# WATEREUROPE ENGINEERING REPORT

## Table of Content

List of Tables.....	4
List of Figures.....	5
List of Equations.....	6
Part one.....	7
1. Introduction.....	7
2. Method of approach.....	7
2.1 Discharge data.....	8
2.1.1 Flood Frequency Analysis (FFA).....	8
Gumbel method.....	8
Normal distribution.....	9
Regression Analysis.....	10
2.1.2 Hydrograph generation.....	11
2.2 Rainfall data.....	11
2.2.1 IDF Curves.....	11
2.2.2 Rainfall generator.....	12
2.3 Hydrological Modelling.....	13
2.4 Hydraulic Modelling.....	14
3 Results.....	16
3.1 Return period hydrographs.....	16
3.2 Flood extent – hydraulic modelling .....	18
4 Discussion and limitations.....	21
Conclusion.....	23
Part two.....	24
1. Introduction.....	24
2. Method of approach.....	24
2.1 Uncertainties due to riverbed.....	25
2.1.1 DEM (Digital Elevation Model) .....	25
2.1.2 Cross-section.....	25
2.1.3 Morphology evolution.....	26
2.1.4 Results.....	26
2.2 Uncertainties due to geometry.....	27
2.2.1 Shape and number of cross-section.....	27
2.2.2 DEM resolution.....	28
2.2.3 Results.....	28
2.3 Uncertainties due to input hydrographs.....	29
2.3.1 Results.....	30
2.4 Uncertainties due to sea level.....	31
2.4.1 Results.....	31
2.5 Uncertainties due to roughness.....	32

2.5.1 Results.....	34
2.6 Uncertainties due to weir coefficients.....	34
2.6.1 Results.....	36
2.7 Uncertainties due to theoretical basis.....	37
2.7.1 Results.....	38
2.8 Uncertainties due to temporal simulation time.....	38
2.9 Uncertainties due to flood dynamic effects.....	39
2.10 Uncertainties due to floodplain.....	39
2.11 Uncertainties due to measurement data.....	40
Conclusion.....	41
References.....	42

## List of Tables

Table 1: Mean and standard deviation for each monthly timeseries examined .....	9
Table 2: Initial curve numbers and imperviousness values for the sub-basins in the HEC-HMS model. 14	
Table 3: Adjusted curve numbers and imperviousness values for the sub-basin the HEC-HMS model.. 14	
Table 4: Various crest types with their corresponding coefficients.....	35

## List of Figures

Figure 1: Schematic of the method of approach for producing return period hydrographs .....	8
Figure 2: Graphical analysis of the Gumbel distribution. Observed discharges are represented as black circles with the computed regression line for the Gumbel distribution in purple. The red squares pinpoint the 10, 20, 50 and 100 year return periods. ....	10
Figure 3: Graphical analysis of the Normal distribution. Observed discharges are represented as black circles with the computed regression line for the Normal distribution in purple. The red squares pinpoint the 10, 20, 50 and 100 year return periods. ....	11
Figure 4: 10-year return period hyetograph produced using IDF curves.....	12
Figure 5: 10-year return period hyetograph produced using Rainfall Generator.....	13
Figure 6: Mesh extent for Telemac 2D simulation of return period hydrographs .....	15
Figure 7: Return period hydrographs produced using the Gumbel distribution method .....	16
Figure 8: Return period hydrographs produced using the IDF curve method .....	17
Figure 9: Return period hydrographs produced using the rainfall generator hourly disaggregation method .....	18
Figure 10: Flood extent for the 20-year return period, 3 hours 25 minutes after the hydrograph peak....	19
Figure 11: Flood extent for the 10-year return period, 3 hours 15 minutes after the hydrograph peak....	19
Figure 12: Flood extent for the 100-year return period, 3 hours 44 minutes after the hydrograph peak..	20
Figure 13: Flood extent for the 50-year return period, 3 hours 44 minutes after the hydrograph peak....	20
Figure 14: Estimated 1994 flood event hydrogram at the Napoleon Bridge, taken from Abily et al., (2015). ....	23
Figure 15: Changing the cross-section placement .....	26
Figure 16: Water level evolution as per the change in cross section.....	27
Figure 17: Cross section of the river and possible cross sections of triangular and rectangular shapes ..	28
Figure 18: Water level at different shaped weirs .....	29
Figure 19: Water level at different scenarios .....	30
Figure 20: Difference in water level with the initial hydrograph .....	30
Figure 21: Maximum water level for the last 5 km of Lower var.....	32
Figure 22: Water level as a function of time at different roughness coefficient.....	34
Figure 23: Discharge corresponding to various discharge coefficients .....	36
Figure 24: Wave equations .....	37
Figure 25: Downstream water level resulting from different wave models .....	38
Figure 26: Figures depicting the clarity of the DEMs. ....	40
Figure 27: Cross sections of a section in a river corresponding to 5 m DEM and 75 m DEM .....	40

## List of Equations

Equation 1: Cumulative distribution function of the Gumbel distribution .....	9
Equation 2: Cumulative distribution function of the Gumbel distribution showing alpha.....	9
Equation 3: Cumulative distribution function of the Gumbel distribution showing beta.....	9
Equation 4: Simplified cumulative distribution function of the Gumbel distribution .....	9
Equation 5: Hazen formula .....	9
Equation 6: Normal distribution .....	9
Equation 7: Normal distribution equation with reduced variant.....	9
Equation 8: Regression analysis formula.....	10
Equation 9: Regression analysis formula with reduced variant.....	10
Equation 10: The montana equation .....	11
Equation 11: Honma formula.....	35

# PART ONE

How to produce 10y, 20y, 50y and 100y return period hydrographs estimation and associated flooded areas in the Var Lower Valley?

## 1. Introduction

The Var catchment is situated in the south of France extending from the Southern Alps at 3100m to the Mediterranean Sea at the outlet near the city of Nice. The catchment is 2822km<sup>2</sup> in size with four main tributaries: Var, Esteron, Vesubie, Tinee, fed by an average annual rainfall of 815mm, snowmelt and a shallow alluvial aquifer. The Lower Valley of the Var has undergone significant modification over the last century, largely due to expanding urbanization, which have contributed to changes in the flow regime. Modifications include a reduction in the width of the river from 300m to 200m near the outlet due to construction of Nice Airport, as well as various dam constructions (Bustica et al., 2010). Flooding is a key hazard in the lower Var and understanding the occurrence and effects of such events is vital to developing flood resilience in Nice. One of the main tools for flood-mapping and flood risk analysis is the quantification of flood inundation levels at different return periods. Return periods are a statistical interpretation of the likelihood of an event occurring within any given year. A 10-year return period for example denotes a 10% chance of that event occurring within any given year, whereas a 50-year return period denotes an event with a 2% chance of occurring within any given year.

This project attempts to address how hydrographs can be obtained for different return periods. These hydrographs are the essential input data that define the upper boundary conditions in hydraulic models, a key modelling tool in understanding flood risk to urban areas. For the purpose of this study, return period hydrographs were obtained for 10, 20, 50 and 100-year return period events using a range of statistical and deterministic approaches, capitalizing on the data and time-series available for the Var. The return period hydrographs were curated and subsequently run through a 2D hydraulic model, Telemac, to demonstrate the potential flood extents for each return period event.

## 2. Method of approach

To produce a set of return period hydrographs, two key methods of approach were adopted: one based on discharge data, with a statistical approach and another based rainfall data adopting both a statistical and deterministic modelling approach. Such methods were selected to compare how the availability of different datatypes can affect the production of 10, 20, 50 and 100-year return periods and assess which approaches are most useful and reliable for estimating flooding within the Var Lower Valley. The chosen approaches, methods and models used within this study are highlighted in Figure 1.

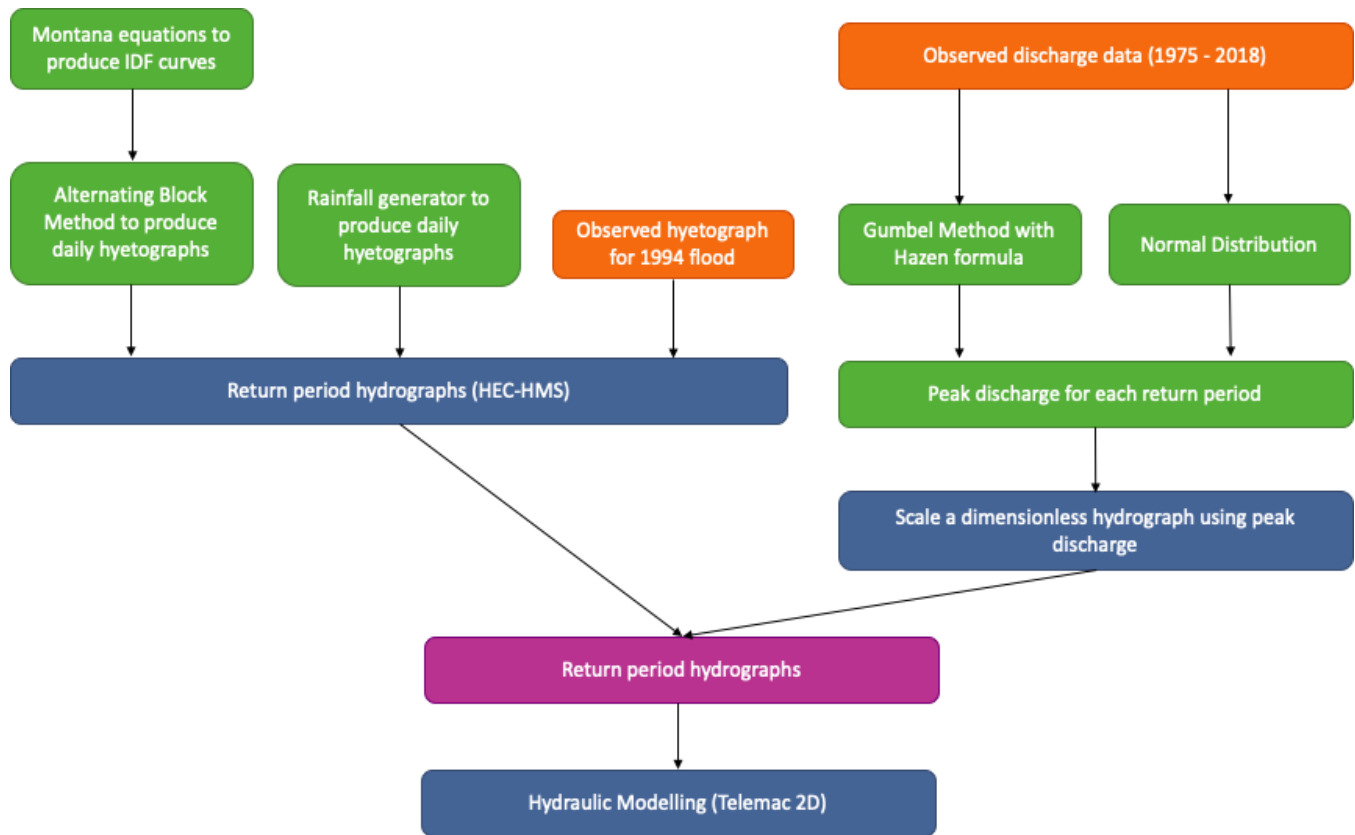


Figure 1: Schematic of the method of approach for producing return period hydrographs

## 2.1. Discharge data

### 2.1.1. Flood Frequency Analysis (FFA)

Flood Frequency Analysis (FFA) is the estimation of how often a specified flood peak discharge will occur. Analysis requires the fitting of a probability distribution model to a sample of annual flood peaks, ideally over a sufficient period of observation (Bhagat, 2017). To estimate the flood peak discharges for the different return periods (10y, 20y, 50y and 100y), two different statistical methods, Gumbel and Normal Law, were employed using an observed daily discharge timeseries for the river Var. The timeseries extended from 1975 to 2018 but with missing data for 2002 – 2005 and 2007.

- **Gumbel method**

The Gumbel distribution is a commonly used statistical method for estimating flood events (Haan, 1997), based on the distribution of extreme events and the use of frequency factors. The cumulative distribution function (cdf) of the Gumbel distribution is expressed in Equation 1:



$$F(x) = \exp \left[ -\exp \left( -\frac{x-a}{b} \right) \right]$$

Equation 1: Cumulative distribution function of the Gumbel distribution

Where  $\alpha$  and  $\beta$  are given by:

$$\alpha = \mu - \beta e$$

Equation 2: Cumulative distribution function of the Gumbel distribution showing alpha

$$\beta = \frac{\sigma\sqrt{6}}{\pi}$$

Equation 3: Cumulative distribution function of the Gumbel distribution showing beta

And assuming a reduced variate,  $u = \frac{x-\alpha}{\beta}$ , for the distribution, Equation 1 can be simplified to:

$$F(x) = \exp (-\exp (-u))$$

Equation 4: Simplified cumulative distribution function of the Gumbel distribution

The peak discharges were ranked in ascending order, and the Hazen formula (Hazen, 1914), shown in Equation 5, was used to obtain an empirical cumulative frequency for each rank, or the probability of non-exceedance.

$$F(x_{[r]}) = \frac{r-0.5}{n}$$

Equation 5: Hazen formula

### • Normal distribution

The Normal distribution defined by the mean ( $\mu$ ) and standard deviation ( $\sigma$ ) was used as an alternative method of distribution for the FFA and follows a similar approach to the Gumbel distribution method. The standard deviation was calculated as per Equation 6, where  $n$  is the size of the sample.

$$\sigma = \frac{\sqrt{\sum (X_i - \mu)^2}}{n}$$

Equation 6: Normal distribution

The mean and standard deviation for each of the periods considered in this study are presented in Table 1.

Table 1: Mean and standard deviation for each monthly timeseries examined

Monthly discharge period	Mean	Standard deviation
1975 – 2018	140	174
1994	293	420.5

The reduced variate,  $u$ , for the normal distribution is given by Equation 7.

$$u = \frac{(x - \mu)}{\sigma}$$

Equation 7: Normal distribution equation with reduced variant

### • Regression Analysis

Following the calculation of the reduced variates,  $u$ , for both the Gumbel and Normal distributions, the reduced variate,  $u$ , for each was analyzed graphically in a plot of discharge ( $\text{m}^3/\text{s}$ ) against the reduced variate. The discharge was obtained from the corresponding non-exceedance,  $F(x)$ , for each reduced variate,  $u$ . Where the reduced variate,  $u$ , is described as:

$$u = -\ln(-\ln F(x))$$

*Equation 8: Regression analysis formula*

Using the assumption that the expression for a given quantile, or non-exceedance,  $F(x)$ , corresponds to the reduced variate,  $u$ , a regression line for both the Gumbel and Normal distributions was computed using the defining parameters for each distribution;  $\alpha$ ,  $\beta$  and  $\mu$ ,  $\sigma$ , respectively. This regression line was then used to relate discharge to reduced variate and extrapolated to estimate the peak discharge for the probability of non-exceedance,  $F(x)$  relating to the 10, 20, 50 and 100-year return periods. The return period ( $T$ ) of an event is defined as the inverse of the occurrence rate,  $1 - F(x)$ , Equation 9.

$$T = \frac{1}{1 - F(X_i)}$$

*Equation 9: Regression analysis formula with reduced variant*

The regression line for each distribution was then compared to the observed discharges for the reduced variate. As shown in Figure 2, and Figure 3 the Gumbel distribution offers the best method for the FFA,

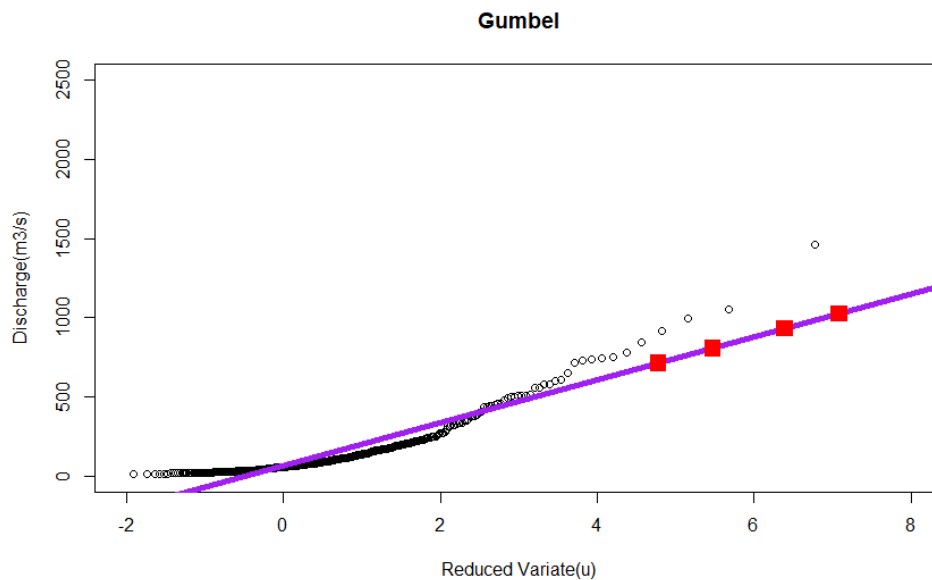


*Figure 2: Graphical analysis of the Gumbel distribution. Observed discharges are represented as black circles with the computed regression line for the Gumbel distribution in purple. The red squares pin-point the 10, 20, 50 and 100 year return periods.*

as the extrapolation of the reduced variate and discharge relationship is more closely aligned to the observed values than approximated by the Normal distribution.

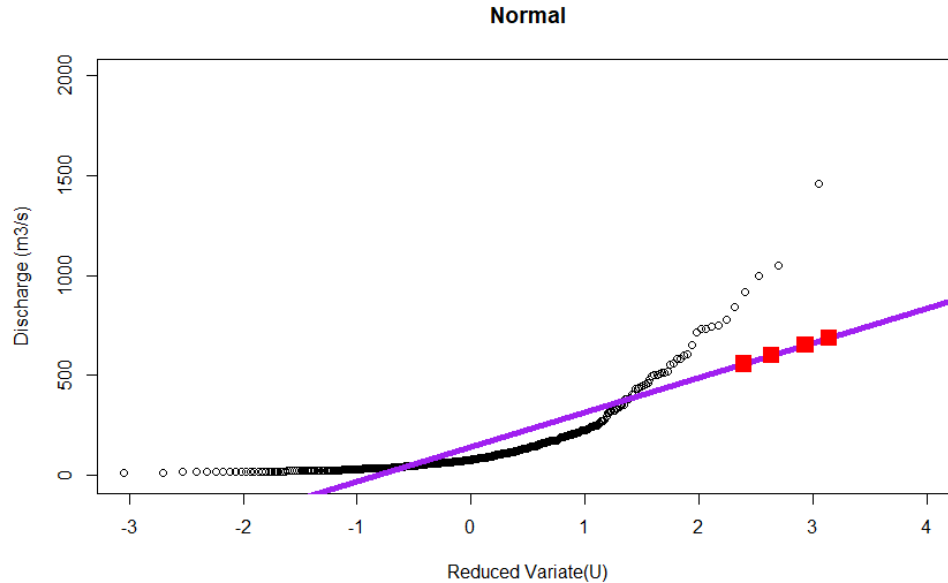


Figure 3: Graphical analysis of the Normal distribution. Observed discharges are represented as black circles with the computed regression line for the Normal distribution in purple. The red squares pin-point the 10, 20, 50 and 100 year return periods.

As such the values obtained for the 10, 20, 50 and 100-year return periods using the Gumbel approach were used in subsequent analysis.

### 2.1.2. Hydrograph generation

The peak values for each return period obtained using the Gumbel distribution were used to scale a unit hydrograph to produce a set of return period hydrographs for the Var lower valley. The unit hydrograph was derived from discharge data for the Var.

## 2.2. Rainfall data

### 2.2.1. IDF Curves

Intensity-Duration-Frequency (IDF) curves relate rainfall intensity with their duration and frequency of occurrence. They are commonly used for stormwater management and are derived from historical annual maximum data (Overeem et al., 2008; Tfwala et al., 2017). The Montana equation (Equation 10) which related intensity (I) to duration was used to produce a set of IDF curves.

$$I = aT^{(-b)}$$

Equation 10: The montana equation

The coefficients  $a$  and  $b$  are local to the Var and were obtained from Meteo France where they had been calculated through statistical methods on measured data from 1966 – 2012; they are specific for different return periods.

To obtain a 24-hour design hyetograph for each return period, the alternating block method adopted. The purpose of the alternating block method is to construct storm hyetographs with the largest rainfall depth at the centre of the storm; rainfall events of decreasing depth are then located to the right and left of the storm peak, alternating until the hyetograph is complete (Butler & Davis, 2011). Values for each hour were obtained from the IDF curve, dividing  $T$  by the time interval,  $\Delta t$ , to obtain estimates for rainfall intensity at each duration  $\Delta t$ ,  $2\Delta t$ ,  $3\Delta t$ , etc. which were subsequently used to calculate the rainfall depth. The hyetographs produced for each return period were then used as input data into HEC-HMS for hydrological modelling.

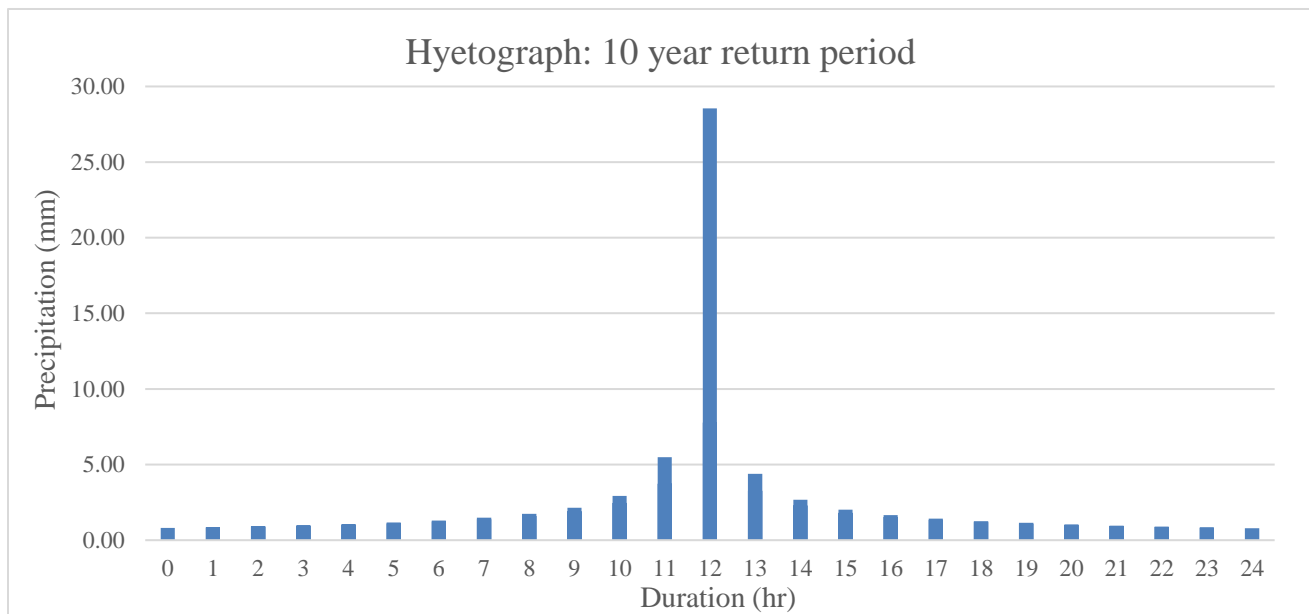


Figure 4: 10-year return period hyetograph produced using IDF curves

### 2.2.2. Rainfall generator

A rainfall generator, set-up for the Var catchment (Newcastle University, n.d.) was adopted as an alternative method for generating storm hyetographs based upon a limited dataset. Two methods of approach were taken using the rainfall generator:

1. The first took the average rainfall timeseries from the 1994 rainfall event as input data and used the hourly disaggregation function within the tool to disaggregate the event into a 24-hour unit hyetograph with the same distribution properties as the original event.

2. The second approach used the pre-defined hourly disaggregation models: Triangular, Back-Loaded, Front-Loaded and Non-Linear and adjusted the time of peak to produce a set of example unit hydrographs for each disaggregation model with peak events at hours 5, 10, 15 and 20 to assess how the distribution of rainfall throughout the storm event affected the resultant event hydrographs.

Each unit hyetograph obtained from the rainfall generator hourly disaggregation function was converted into a hyetograph corresponding to the desired return periods: 10, 20, 50 and 100 years. These hyetographs were then used as input data into HEC-HMS for hydrological modelling.

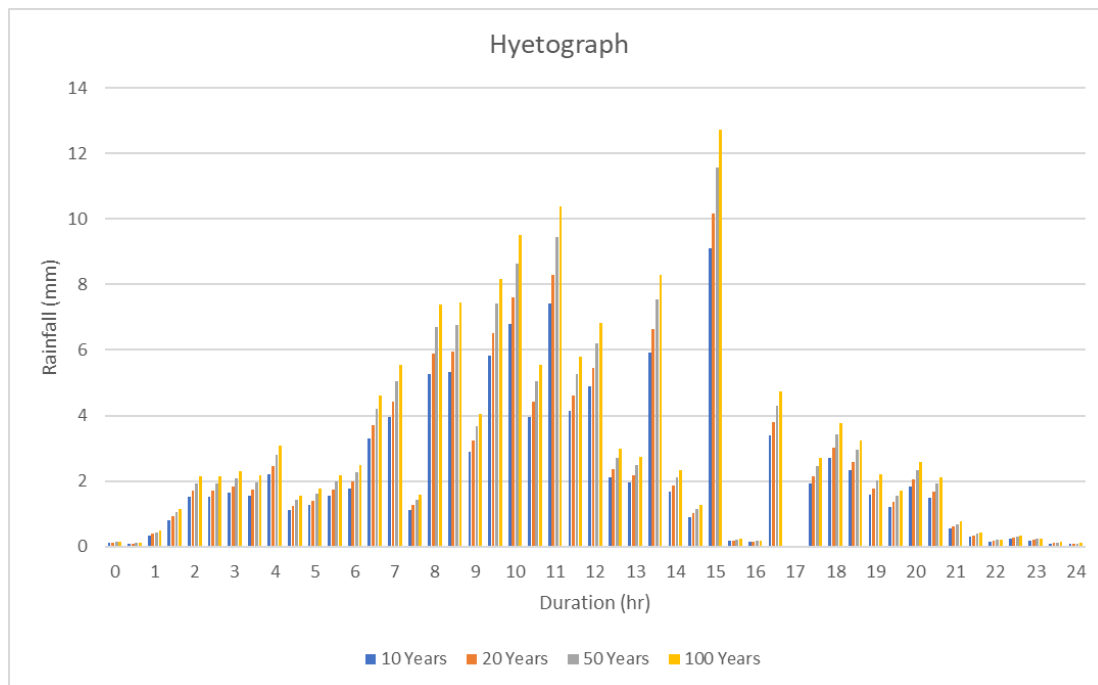


Figure 5: 10-year return period hyetograph produced using Rainfall Generator

### 2.3. Hydrological Modelling

To produce return period hydrographs from the rainfall data, the hydrological model HEC-HMS was selected. HEC-HMS is a physically based, semi-distributed model that is capable of simulating rainfall-runoff processes for large river basins and flood events (Tassew et al., 2019). HEC-HMS was configured to include five sub-catchments, three junctions and three reaches to represent the Var catchment. A single precipitation gauge was introduced, assuming an even distribution of rainfall across the catchment using the input hyetographs over the 24-hour period at using 30 minute intervals. Each of the sub-basins were initially given the curve numbers and imperviousness values shown in Table 2 and a peak discharge of 61.13m was initially obtained. As this value was not realistic, the curve numbers and imperviousness values were adjusted as shown in Table 3 to obtain more realistic outputs.

Table 2: Initial curve numbers and imperviousness values for the sub-basins in the HEC-HMS model

Sub Basin	Curve Number	Imperviousness
Upper Var	77	20
Tinee	75	21
Esteron	72	13
Vesubie	73	17
Lower Var	72	24

Table 3: Adjusted curve numbers and imperviousness values for the sub-basin the HEC-HMS model

Sub Basin	Curve Number	Imperviousness
Upper Var	60	18
Tinee	60	19
Esteron	60	13
Vesubie	60	15
Lower Var	60	22

## 2.4. Hydraulic Modelling

Simple hydraulic modelling was carried out using Telemac 2D to display the flood extent for each of the return period hydrographs. Telemac-2D solves using the depth-averaged Navier-Stokes equation utilizing both Finite Element (FE) and Finite Volume (FV) formulas. These require a spatial representation of the domain as defined using a computational mesh. For the purpose of this study, a mesh of 5m resolution for the minor riverbed, 50m for the major bed and up to 400m for the rest of the model was defined covering the area from the La Manda bridge to Nice airport (Figure 6). Due to time constraints, modelling was only carried out using the return period hydrographs produced from the Gumbel distribution hydrographs.

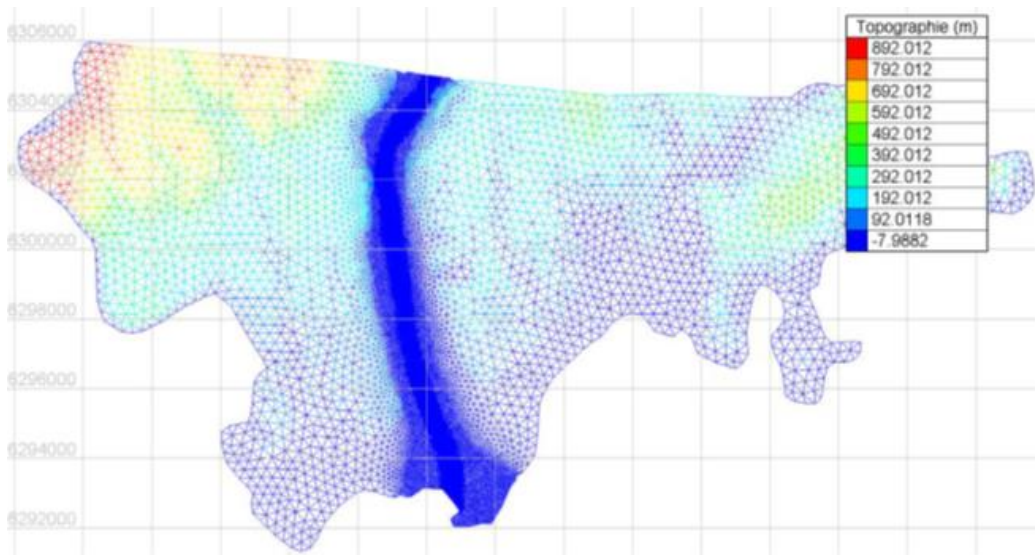


Figure 6: Mesh extent for Telemac 2D simulation of return period hydrographs



### 3. Results

#### 3.1. Return period hydrographs

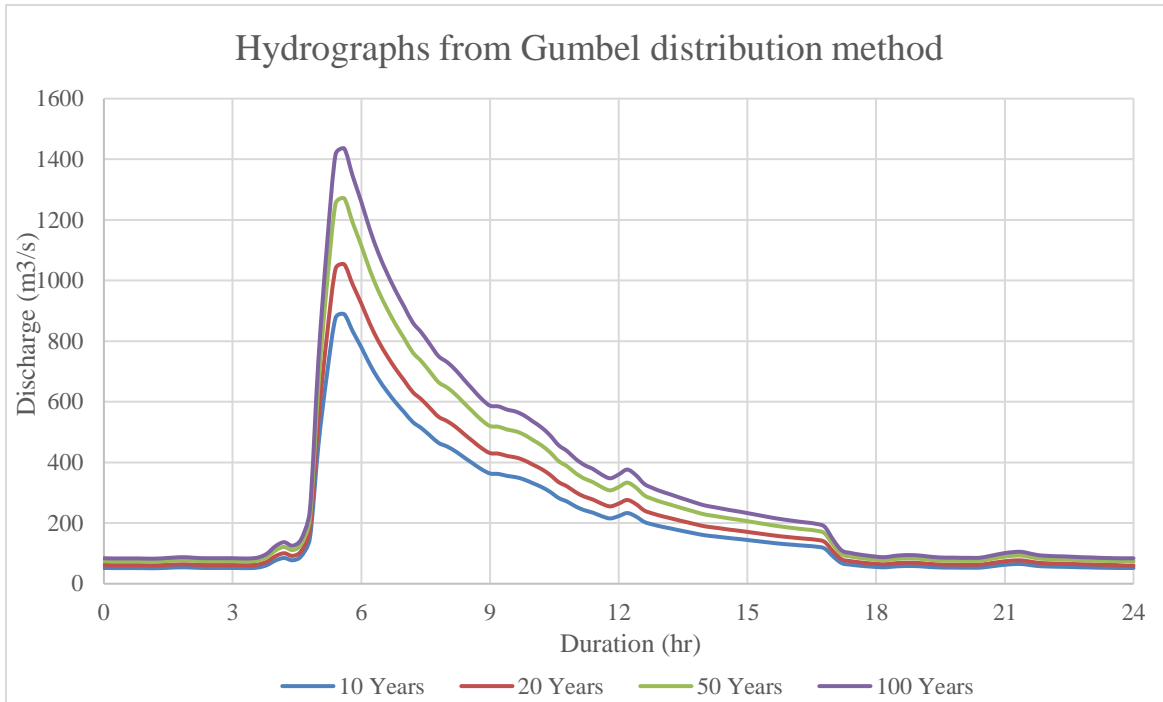


Figure 7: Return period hydrographs produced using the Gumbel distribution method

Return period hydrographs for both the IDF curve method and the rainfall generator disaggregation method are presented in Figure 5, Figure 6 and Figure 9 7. The hydrographs produced using the Gumbel distribution are for a 24-hour period only and so are not necessarily comparable to those produced using HEC-HMS. The Gumbel distribution return period hydrographs show a flashier response of the lower Var and as non-modelled hydrographs, each return period hydrograph is simply the same response at a different magnitude. However, for all of the return period hydrographs, the peak flows much lower than expected for storm events.



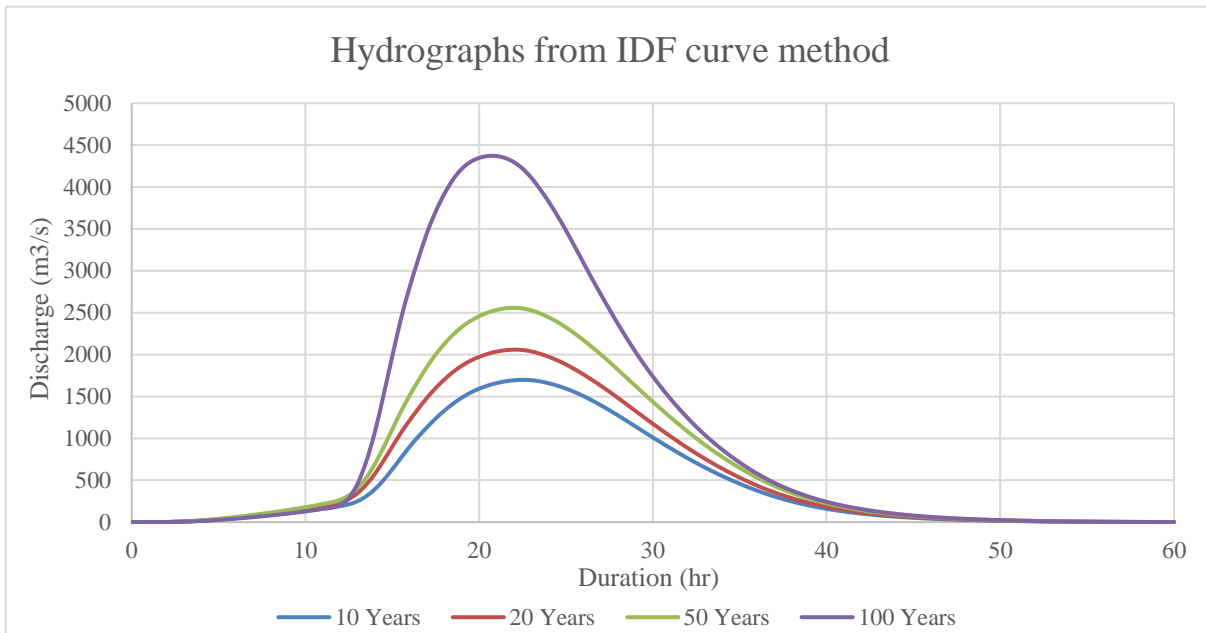


Figure 8: Return period hydrographs produced using the IDF curve method

Both the IDF curve and rainfall generator methods give similar magnitude peaks for the 10, 20 and 50-year events, with a difference of  $1277\text{m}^3/\text{s}$  in the magnitude of the 100-year event hydrograph. More interestingly, the storm peaks of the hydrographs produced using the IDF appear sooner into the simulation than the storm peaks of the hydrographs produced using the rainfall generator method, with a difference of 1 hour for the 10, 20 and 50 year return periods, and a difference of 2.5 hours for the 100 year return period event.

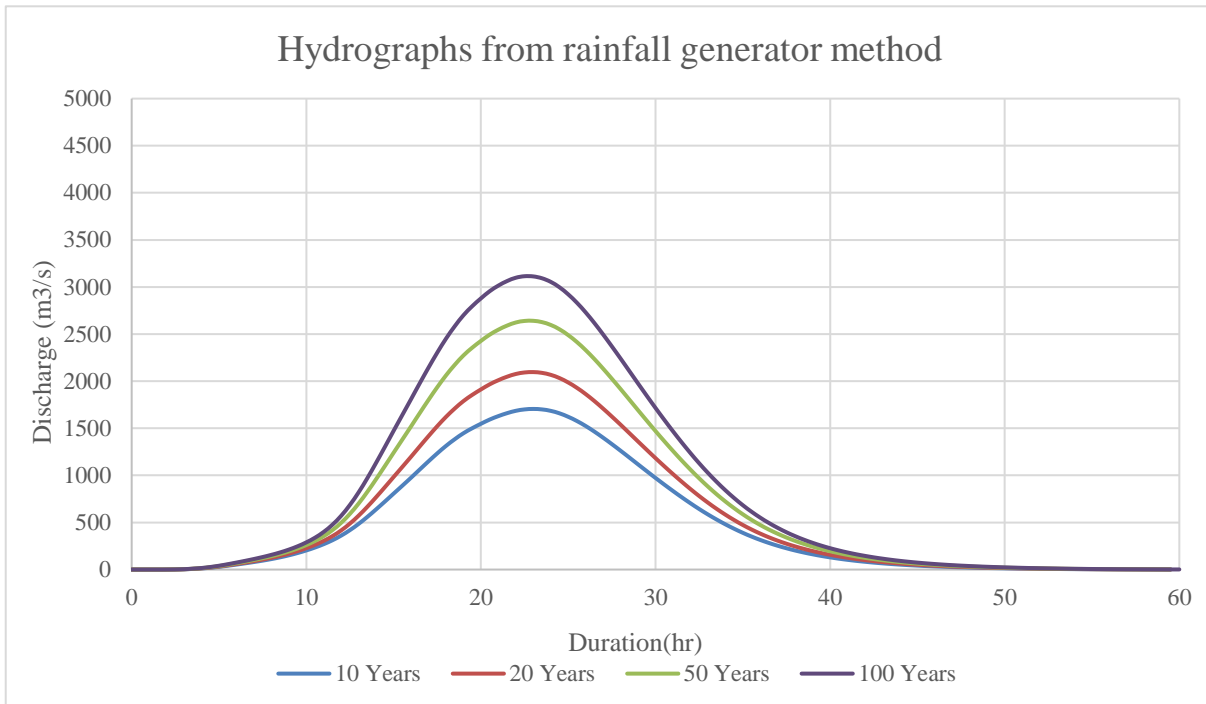


Figure 9: Return period hydrographs produced using the rainfall generator hourly disaggregation method

### 3.2. Flood extent – hydraulic modelling

A snapshot of the flood extent for each of the return period hydrographs produced using the FFA method are shown below in Figure 11, Figure 10, Figure 13 and Figure 12. With each increasing return period, there is additional flooding and depth of flooding in the city of Nice, north of Nice airport, with some flooding on the runways too. Isolated spots of flooding occur at the upper end of the Lower Var with the 50 and 100-year return period events, although flooding levels are at less than 1m here. The maximum flood extent occurs with the 1 in 100-year return period event, as expected, with 1.3m of flooding to the north of Nice airport in the business district.

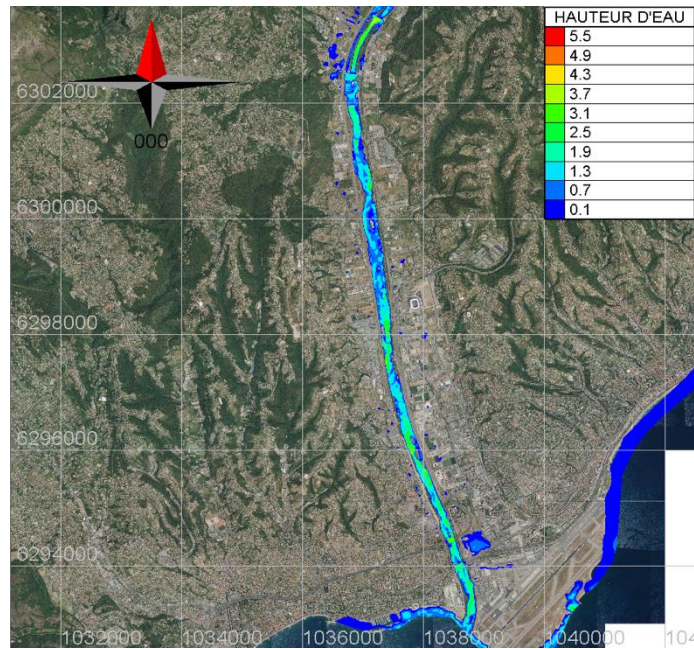


Figure 11: Flood extent for the 10-year return period, 3 hours 15 minutes after the hydrograph peak

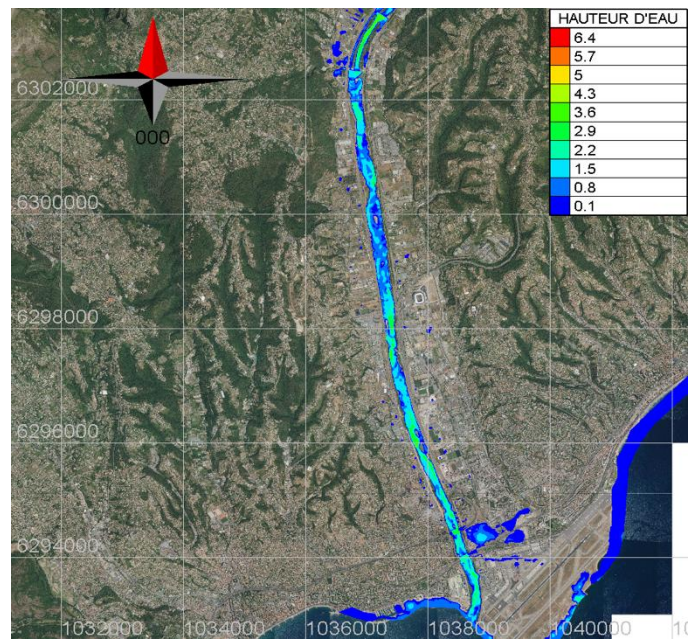


Figure 10: Flood extent for the 20-year return period, 3 hours 25 minutes after the hydrograph peak



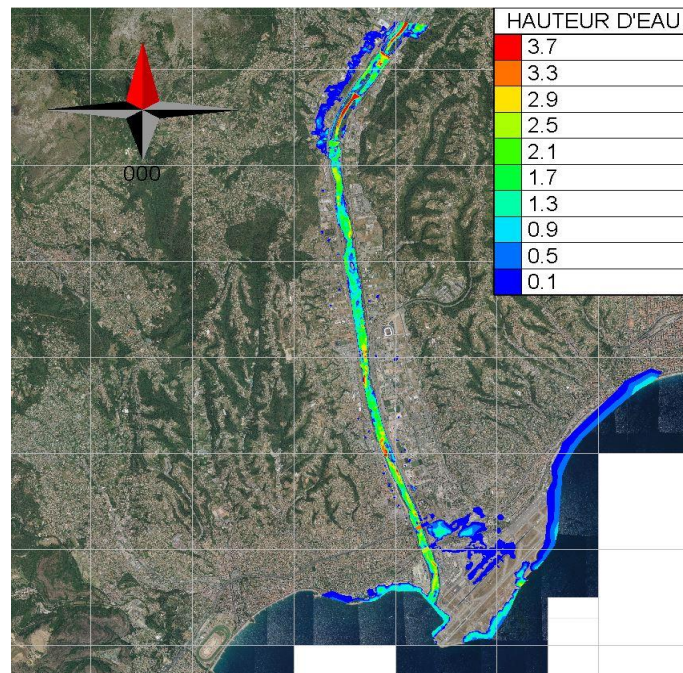


Figure 13: Flood extent for the 50-year return period, 3 hours 44 minutes after the hydrograph peak

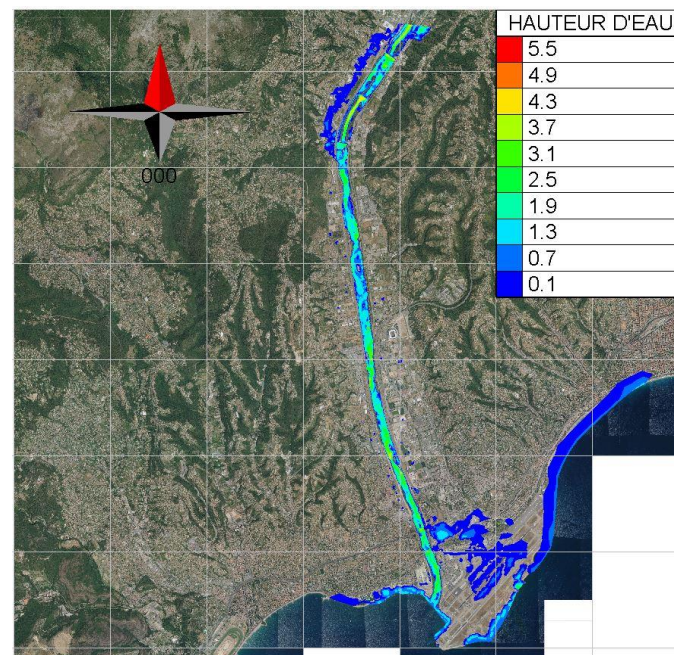


Figure 12: Flood extent for the 100-year return period, 3 hours 44 minutes after the hydrograph peak

#### 4. Discussion and limitations

The results highlight the importance of producing return period hydrographs for hydraulic modelling, flood inundation mapping and risk management for the city of Nice. Particularly for the more extreme, 50 and 100-year events, flooding has the potential to cause significant damage and disruption to the business district and Nice airport, with additional flooding damage in the upper Lower Var. Several methods were adopted for the initial curation of return period hydrographs, making use of the data available, where possible, and allowing for analysis of the most suitable methods. All the methods were conducted under limited time conditions, and so the results produced for all three methods, and for the hydraulic modelling, are not necessarily a true reflection of the potential of each of the methods.

For the statistical approaches where the Gumbel and Normal distribution models were applied to a discharge timeseries, the results were much lower than what would be expected for all three of the return periods, and thus so was the flood extent for the Var. The Normal distribution, as expected, was not suitable for the estimation of peak events and so the Gumbel distribution was used. One possible limitation is that Gumbel's distribution is commonly most appropriate on catchments where there is no major tributary (Bhagat, 2017). In the case of the Lower Var, there are three additional tributaries (in addition to the Var) into the lower portion of the catchment, and thus this distribution may not be the most suitable as all the tributaries have the potential to affect the flood peak. Further to this, the dataset used to carry out the FFA was incomplete at 88% completeness. Although there was still a good amount of data for the FFA, it is possible that extreme values occurring in those missing years could have contributed to lower estimates for the peaks for each return period. In addition, this method is a statistical extrapolation of the observed data for which there was only 30 years' worth of initial data. When trying to obtain peak estimates for return periods greater than the length of the time series analyzed, there is likely to be significant uncertainty as statistically speaking it is unlikely that such extreme events would have occurred in this time frame (REF). The issues with extrapolating a shorter time series can be seen in Figure 2 where the extrapolated line for the Gumbel distribution is a clear underestimation compared to the extreme observed values with high reduced variates. This is a common issue when using the Gumbel distribution for events with small probabilities of exceedance, as it yields the smallest possible quantiles (Koutsoyiannis, 2003). Given this, it is recommended that a longer, more complete timeseries should be analyzed with additional tests of other distributions. Some distributions that may be more suitable for analysis are the exponential distribution, 2-parameter lognormal distribution (Markiewicz et al., 2015) and the three-parameter Frechet distribution (Koutsoyiannis, 2003).

For the IDF Curve and rainfall generator approaches, it was assumed that rainfall would be equal across the catchment. As such, an average input was provided to one gauge set within the catchment. This assumption is appropriate for small catchments (Faures et al., 1995; Van de Beek et al., 2010), however, as a large catchment, it is unlikely to be suitable for the Var, particularly given the topographic and geographic variation within the catchment. As such, this method led to an overestimation peak discharge

when the data for each rainfall return period was fed into the HEC-HMS model. This is not surprising, given that rainfall distribution is likely to be highly variable throughout the Var catchment, even under storm conditions where high return period rainfall events are most likely to occur either locally over the mountains in the Upper Var, or along the coastline near the outlet of the Var. In the latter, the rainfall is more likely to result in pluvial flooding as opposed to the fluvial flooding which is assessed within this report. As a result of this assumption, the parameters for imperviousness and curve number had to be recalibrated so that the simulated hydrographs were comparable to known past extreme events, such as the 1994 event. For additional study, it is recommended that separate hyetographs are used across the five known raingauges within the Var catchment to offer a more realistic picture of the effect of the different rain events. Moreover, it is well known that for any given return period flood, the return period of the rain events is highly variable and specific depending on the duration and location of the event, with many cases of lower return periods of rainfall producing high return period flood events (Viglione & Blöschl, 2008). In other words, not all areas of the catchment experiencing a 100-year rainfall event to produce a 100-year flood event, particularly for large catchments with several main tributaries such as the Lower Var. With this considered, if adopting the approach of separate hyetographs and additional raingauges for further analysis, design storms of different intensities should be considered across the different gauges, to produce a range of hydrographs for further analysis.

In this study, the results of the simple hydraulic modelling are of limited use as they are based upon the flawed Gumbel FFA method. Furthermore, due to time constraints, limiting the testing of different boundary conditions and initial conditions in Telemac, flooding of the sea occurred. To overcome this for future studies, the lower boundary conditions for the Lower Var should be set further into the sea to allow for drainage.

Overall, the IDF curve and rainfall generator approaches both showed success in the production of return period hydrographs for the Lower Var. The hydrographs obtained through both methods are generally in agreement in terms of magnitude, with differences in the timing of the event. The only key difference in magnitude is for the 100-year return period event where the IDF curve approach gives a peak discharge of 4300 m<sup>3</sup>/s and the rainfall generator a peak discharge of 3100 m<sup>3</sup>/s. When comparing to the peak magnitude of the 1994 flood event, given to be 3680m<sup>3</sup>/s (Figure 14) it can be said that the rainfall generator approach is a closer estimation of a 100-year return period event. However, it must be noted that shape of the hydrographs produced are not necessarily a good representation of the response to the Lower Var in a storm event. In this instance, it can be said that the rainfall generator may be a more suitable method to produce return period hydrographs, however, more work should be done to test different intensities and durations of rainfall events for subsequent hydrological modelling. This would enable a wider range of return period hydrographs for different duration events to be produced for the Lower Var.



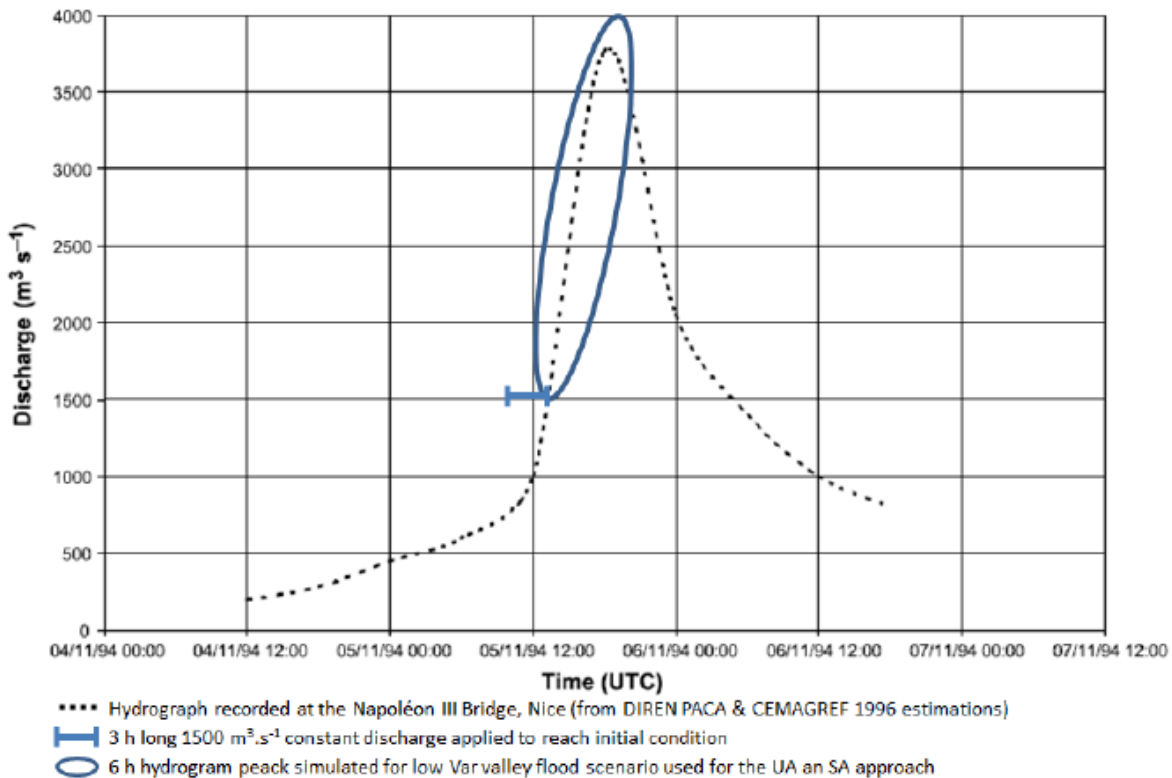


Figure 14: Estimated 1994 flood event hydrograph at the Napoleon Bridge, taken from Abily et al., (2015).

## Conclusion

To produce a set of return period hydrographs for the Lower Var, there are several methods of approach that can be taken depending on time and data availability. In the absence of reliably long time series, the IDF curve approach can be used to obtain a fairly reasonable set of return hydrographs in a short space of time. Statistical methods have potential to be useful, however, the distributions, Normal and Gumbel that were evaluated in this report proved unsuitable in the curation of return period hydrographs for the lower Var. Additional work could be carried out to assess other distributions for a statistical approach, however, other uncertainties due to gaps in the discharge time-series for the Lower Var mean that this type of approach is unlikely to be the best solution. Further to this, when considering approaches for other catchments, discharge data is typically limited or less available than rainfall data. In this report, the use of rainfall data and the curation of unit hyetographs for hydrological modelling is determined to be the better method for return period hydrograph generation. Further research should be carried out to develop hyetographs for each of the gauging stations in the Var catchment so that a more accurate distribution of rainfall could be used as an input to a hydrological model such as HEC-HMS.

# PART TWO

What are the uncertainties in 1D hydraulic modelling for the Var lower valley (riverbed, floodplain, input hydrographs, roughness, weir coefficients, geometry, sea level? ...)

## 1. Introduction

Quantitative estimation of error present in data is understood as uncertainty (Vision learning, 2008). Either through systematic error and/or random error, every measurement contains uncertainty. It is crucial for scientific investigations to acknowledge uncertainty. Uncertainty provides the extent to which researchers can be confident in their data. It indicates the range of possible values within which true value lies. (Carleton, 2018).

Uncertainties in hydraulic modelling can be described as the deviation of obtained results from the actual results due to various parameters and assumptions of the modelling platform. This report explains the uncertainties in 1D hydraulic modelling for the Var lower valley.

## 2. Method of approach

To understand and explain the uncertainties in 1D hydraulic modelling, Mike 11 was used as the modelling platform. The uncertainties in the hydraulic modelling of the Var lower valley was analyzed mainly by varying the following parameters in Mike 11:

1. Riverbed
2. Geometry
3. Input hydrographs (Upper boundary conditions)
4. Sea level (Lower boundary conditions)
5. Roughness
6. Weir coefficients
7. Theoretical basis
8. Flood plain
9. Measurement data
10. Temporal simulation time
11. Flood dynamic effects

Out of the parameters listed, 1-7 were modelled and the rest are explained theoretically.



## 2.1 Uncertainties due to riverbed

The riverbed is defined by a topography in the DEM and by the cross sections in 1D model. Some of the factors that create the riverbed uncertainty are explained below namely:

### 2.1.1 DEM (Digital Elevation Model)

The riverbed uncertainties coming from the DEM result from the DEM resolution. In fact, a DEM with a poorer resolution (meaning with bigger distance between its points) will generate more interpolations in the topography and will create bigger uncertainties. The DEM resolution will mostly depend on the method used to measure the real topography (satellite, laser scan, Geometrician measure etc.).

The uncertainties coming from the DEM resolution in the riverbed can be modelled by using different DEM with different resolution size.

### 2.1.2 Cross-section

In a 1D model, the riverbed is described using cross sections. For a series of cross sections to be more accurate, each cross section must follow these rules:

- Be approximately perpendicular to the stream at the point where it intersects it
- Only intersect the main channel once
- Not cross another cross-section

Nevertheless, if there is a confluence of a tributary with the main channel, it may not be possible for the cross section to be perpendicular to both channels, therefore the riverbed may not be accurately represented at confluence. This can then act as the source of uncertainty. The distance between the cross section will also affect the uncertainties of the result as cross sections far apart will generate more topography interpolation between sections.

The uncertainty coming from the position of the cross sections can be modelled by varying the number of cross sections describing the river or changing the placement of these cross sections by putting fewer cross sections around the singularities (weirs, turns...).

### 2.1.3 Morphology evolution

Finally, the changes in the river morphology due to sediment transport during the years or during special events adds an uncertainty factor as the topography used to model one event may not have been measured at the time of the event and may indeed not be the correct one.

A DEM with a small resolution, a poor number of cross sections or a bad cross section placement will make singularities of the riverbed disappear from the model as they may not be represented by the sections. This will influence the result flow as it will not show the impact of the singularity on the flow.

There is no easy way to model the morphology evolution of the riverbed on the long time. For an event, it is possible to consider the sediment transport. But for a long-term evolution, the only way would be to use different DEM measured at different times (not possible here and rarely possible elsewhere).

To model the riverbed uncertainty, the placement of the cross section around the weirs of the model were modified. The test was done with the following distances: 1, 20, 50, 200, 150, 200, 250, 300 and 400 m. Interpolation was then performed from existing positions to the chosen distances, which are before and after each weir. The cross sections that were too close to the weirs were gotten rid of if needed.

### 2.1.4 Results

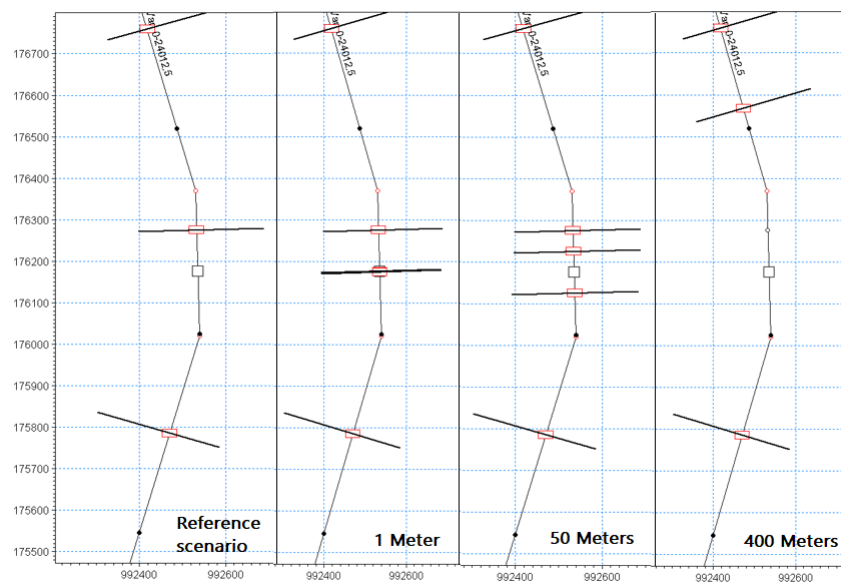


Figure 15: Changing the cross-section placement

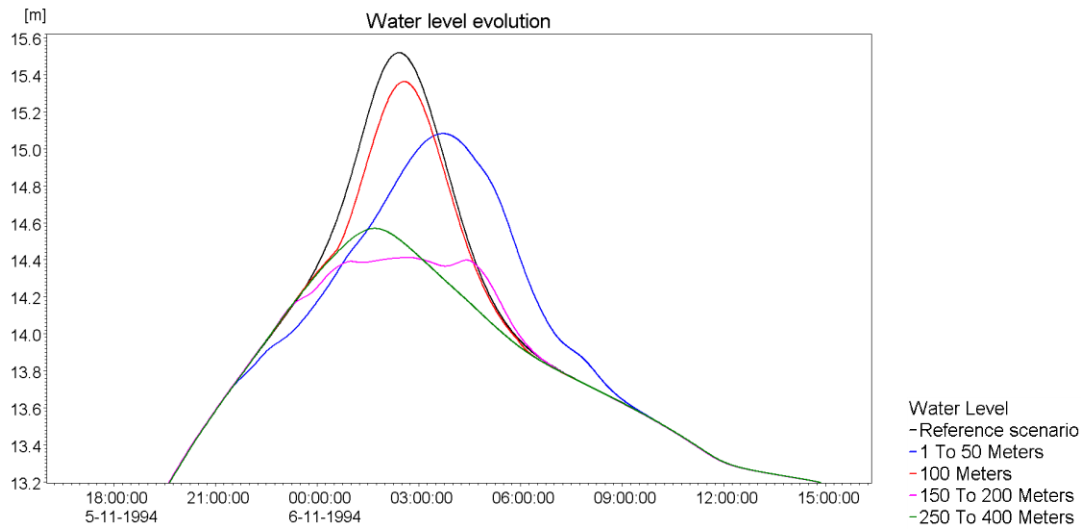


Figure 16: Water lever evolution as per the change in cross section

From 1 to 50 m, the cross sections were placed on the crest of every weirs. There were no significant changes in the peak and shape of the water level. At 100 m, the cross sections for all the weirs except one were still on the crest. The curve is the smoothest with highest peak. From 150 to 200 m, the cross sections were at the bottom of the weir. The peak has disappeared, and the shape of the curve has been modified which can be the result of a rapid elevation of water due to the presence of the weir. From 250 to 400 m, bottom level of the cross sections was higher than the crest of weir, therefore, the water is only going downstream to the point where when crossing the weir, its impact on the structure is strongly minimized. The curve is smooth, and the result is stabilized.

Using a DEM with proper resolution for the study area is an excellent option to avoid uncertainties due to riverbed. Additionally, it is also important to have enough cross sections and correct placement of them in the model. It is also highly recommended to have cross sections around singularities that cause changes in the water flow behavior to make sure it is correctly represented.

## 2.2 Uncertainties due to geometry

This type of uncertainty is associated with the shape of the cross section of rivers. Sources of uncertainties due to geometry are:

### 2.2.1 Shape and number of cross-section

Shape of the cross section is a source of uncertainty due to geometry. The shape used to simulate a 1D model should sufficiently represent the real cross sections. The number of the points representing the cross section is also an important factor contributing to uncertainty. Higher number is a better reflection of the real cross section.

## 2.2.2 DEM resolution

DEM resolution is another source of uncertainty in representing the geometry. Low resolution DEM represents the shape of the cross section very smoother while the higher resolution captures all the details of the cross sections.

To model the uncertainty in the geometry, two types of cross section shapes were considered in Mike 11. The first type is triangular cross section, an extreme case where just three points represent the shape. And the second type is the trapezoid shape, considered as the less complex shape. All the cross sections along the river were converted to two different shapes. To convert the cross section to triangular one, points of cross section in the cross-section file were reduced just to three points: the left and right bank and the lowest point of the cross section. To change the cross section to trapezoid shape, four points were selected, the left and right bank, the lowest point in the first and second half of the cross section.

## 2.2.3 Results

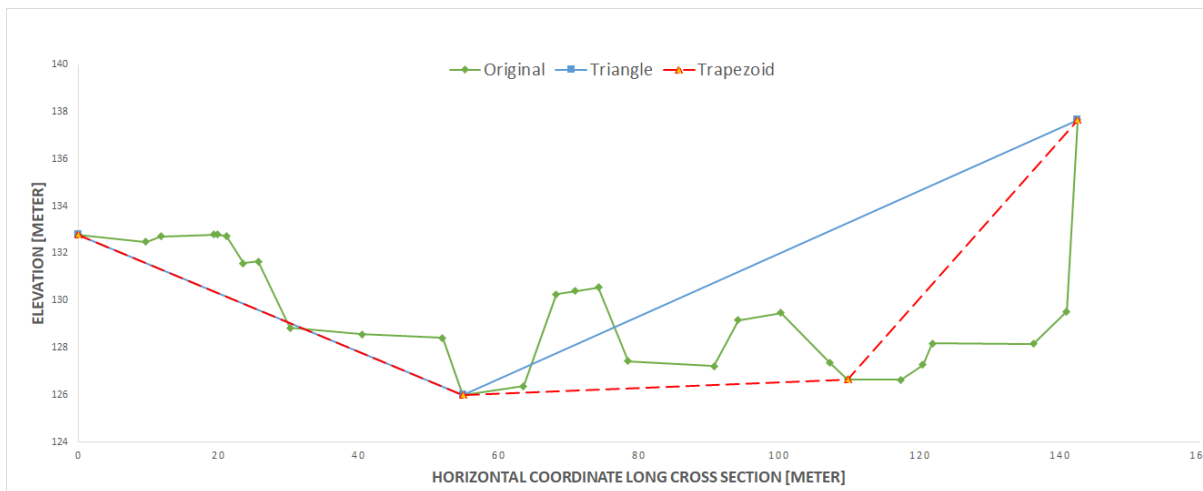


Figure 17: Cross section of the river and possible cross sections of triangular and rectangular shapes

The number of points representing the shape of cross section is a source of uncertainty in hydraulic modelling. Resolution of DEM data can be another source of uncertainty to obtain cross section data. Low resolution DEM provides smoother and less detailed data whereas high resolution DEM provides greater detail.

## Water level in different shapes of cross sections

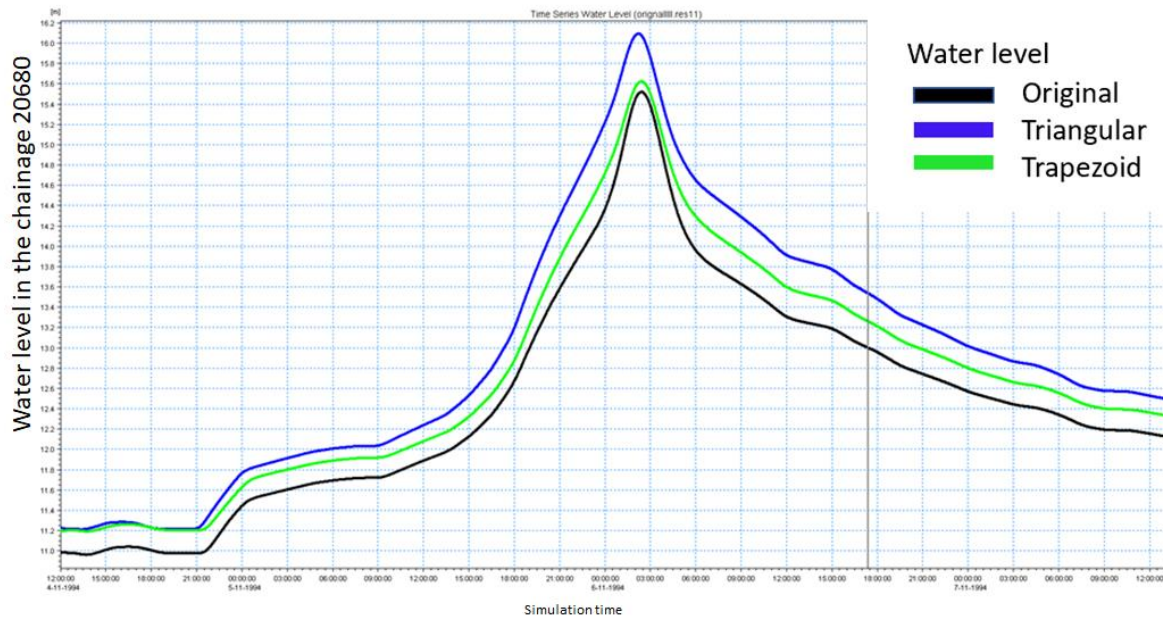


Figure 18: Water level at different shaped weirs

### 2.3 Uncertainties due to input hydrographs

The measurement of flows in a river is the main source of uncertainty in model input hydrographs. Indeed, this uncertainty is directly related to the accuracy of the measurement. To obtain the flow of a river, the water level in each section is regularly measured. It is then possible to convert the recorded water level into flow using the calibration curve. The calibration curve (relationship between water height and flow at a given site), is mainly constructed from measurements that have been made over a range of heights. Generally, the number of measurements is insufficient or insufficiently distributed and the calibration curve must be extrapolated at its extremities: to cover the needs of flood forecasting and water resources (low water level). An assessment carried out by Cemagref (2005) concerning 325 stations in the Rhône Méditerranée Corse (RMC) hydrographic basin showed that the hydrometric stations are relatively well gauged up to a return period of less than 2 years, and that only 9% of these stations have gauges beyond the ten-year flood. Flood forecasting needs extend well beyond these return periods, especially in the case of red alert. By changing the data in a hydrograph, the amount of water in the domain also changes. This then affects not only the extent of the simulated flood but also the water heights. Larger flows over a longer period lead to a larger extension and higher water heights.

The simplest solution to model this uncertainty is to perform several simulations with different hydrographs. To test the sensitivity of this input, two new hydrographs were produced from the hydrograph of the 1994 flood: one hydrograph corresponding to the base hydrograph at which the flow



values are decreased by 10% and one at which the flow values are increased by 10%. Based on the three models carried out, it was possible to compare whether an error in the measurement of the flows of the order of plus or minus 10% induced a greater or lesser difference in the extension of the flood and the simulated water heights.

### 2.3.1 Results

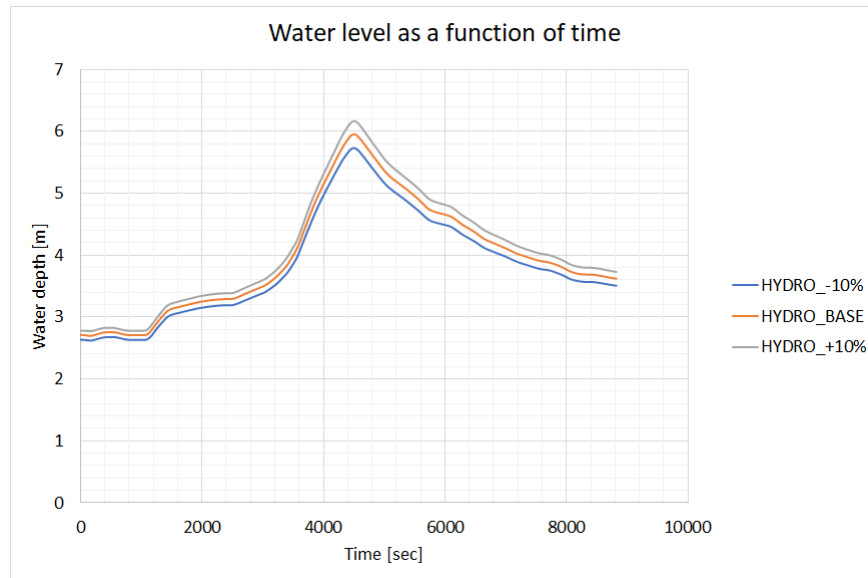


Figure 19: Water level at different scenarios

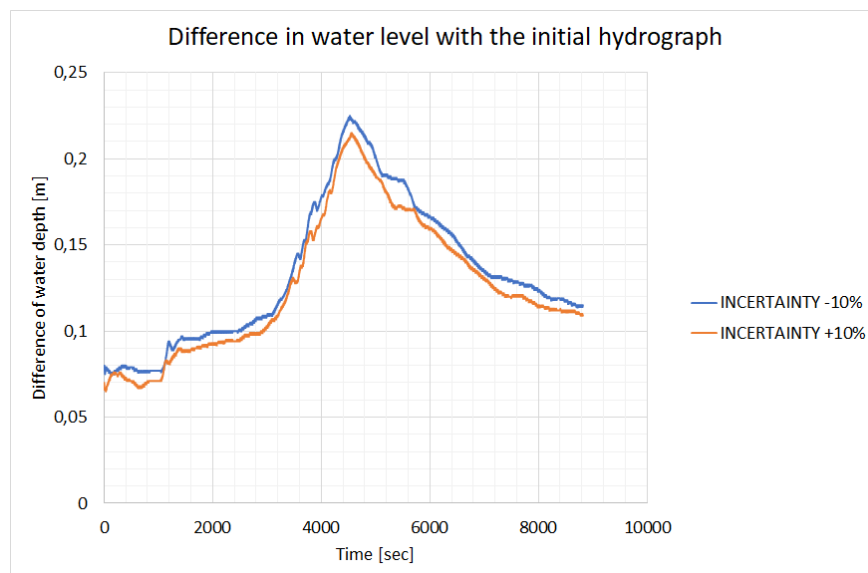


Figure 20: Difference in water level with the initial hydrograph

When the simulations were performed, it was expected that the hydrographs would have a significant impact on the water heights. But it can be observed from the results above that a 10% increase or decrease in flows does not significantly change the simulated water heights.

There are several methods to determine whether the hydrographs used in model inputs are valid. However, these methods are more qualitative in nature. Nevertheless, to get ideas of the uncertainties, it can be observed whether the hydrographs appear to be consistent and with no outliers. It is also possible to use calibrated hydrological models to see if the flow values predicted by them are consistent with the flow values of the rain events.

## **2.4 Uncertainties due to sea level**

Sea level is the height of the sea surface above an equipotential surface, called the geoid. The geoid is where the sea surface would come to rest in the absence of tides, water density variations, currents, and atmospheric effects. Sea level varies continuously throughout the day typically due to tidal variation with 2 high tides and 2 low tides. The magnitude of such tides also varies monthly and throughout the year due to the position of the sun with the moon. When the sun and moon are aligned then a phenomenon called ‘super tides’ or ‘spring tides’ occur. As the lower Var terminates in the Mediterranean Sea, the lower boundary conditions for hydraulic modelling are determined by the water-level of the Mediterranean Sea. This presents a large amount of uncertainty due to the diurnal variation in water level thus making it difficult to determine what the lower boundary conditions should be. This is particularly important when considering flood mapping or inundation of the lower Var as the water level at the lower boundary conditions would have implications for overall flood level and water attenuation. Another consideration therefore is the extent of the tidal range within the Var, in other words, at what point in the Var does the effect of the tides no longer persist. The uncertainties caused by the sea level was tried to model by varying the lower boundary condition. That is, water level in the range 0.32 m to 0.56 m.

### **2.4.1 Results**

The variation of the tidal path does not have significant change in the water level upstream. The figure below shows unrealistic tidal changes to demonstrate water level changes upstream.

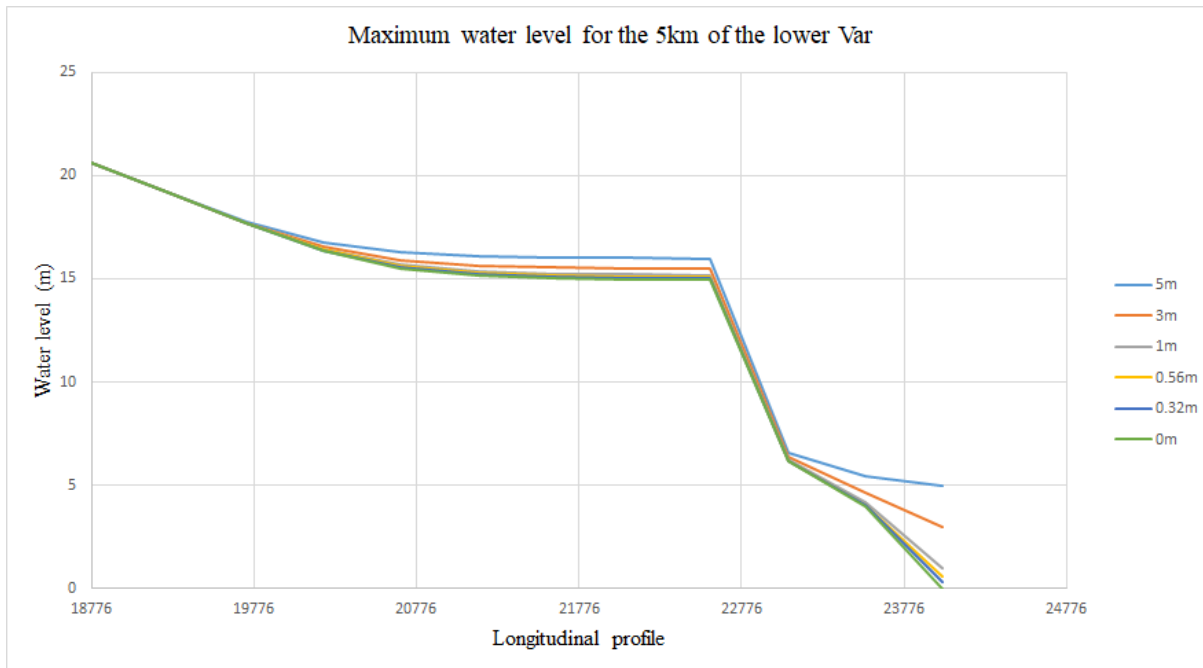


Figure 21: Maximum water level for the last 5 km of Lower var

To account for the uncertainty due to sea level, it is important to consider the maximum and minimum sea level. The quantification of uncertainty due to sea level also depends upon what the modelling is being done for. For example, in case of shipping, we consider minimum sea level to have an idea if the ship keel is immense enough in the water to move and for flood extent, we consider maximum sea level.

## 2.5 Uncertainties due to roughness

Roughness coefficients define the resistance of a channel bed or floodplain to flood flows. Values of roughness for floodplains are typically quite different to the roughness of the corresponding channel bed and banks and should therefore be determined independently to reduce uncertainty (Arcement et al, 1989). Roughness can be input into hydraulic models either as Strickler roughness coefficient ( $K_s$ ) or as Manning's  $n$ -value, depending on the model, where it is used to calculate the discharge as a function of flow depth. Strickler roughness coefficient is taken as the inverse of Manning's  $n$ -value. Roughness is often referred to as one of the two key uncertainties in the literature (Bozzi et al., 2015; Mukolwe et al., 2014) having significant influence on the predicted water levels for applications such as flood forecasting, mapping and design of flood protection. Uncertainty in bed roughness can be attributed to seasonal vegetation growth and depletion, as well as heterogeneity in channel sediment (Vatanchi & Maghrebi, 2019). Yet a key factor in roughness coefficients is their subjectiveness, and at present there is no determinate way to derive the coefficient (Vatanchi & Magherbi, 2019).

Uncertainty due to roughness in a study by Bozzi et al., (2015) was analysed through the use of uniform flow in rectangular channels, and for steady gradually varied flow in real rivers using HEC-RAS and



Monte Carlo simulations. Roughness uncertainty was found to be responsible for output distributions with heavier right tails i.e. if a symmetrical PDF of water level outputs was used, there would be an underestimation of high flows. Another method of approach for assessing uncertainty more simply could be varying by  $\pm 10\%$  and  $\pm 25\%$  for example, as per Wohl (1998), which also used HEC-RAS, where the percentage change in value was compared to the percentage change in discharge from the original simulation.

The uncertainty in roughness in hydraulic modelling manifests itself as a source of error for the rating curves for discharge and stage (Mukolwe et al., 2014), thus resulting in discrepancies between a measure rating curve and hydraulic simulations, both of which are subject to uncertainty (Neal et al., 2009). Where floodplains are present in the area of study, such as within the Lower Var Valley, the uncertainty in Strickler coefficient is likely to be high (Bozzi et al., 2015). Some of the largest discrepancies in discharge for uncertainties in Manning's  $n$  occur where the channel has a relatively low gradient, and a low roughness (Wohl, 1998). This is important when considering the lower Var valley where the gradient of the channel is very low, approximately 0.5 degrees, and outside of the channel bed, the surface roughness is low due to the urban environment on the lower Var flood plain. Other important considerations for the Var Lower valley is the distribution of sediment both spatially and temporally which increases uncertainty when carrying out hydraulic modelling, or model testing using past flood events. Further to this, as a braided river channel, with a large urban floodplain, there is considerable variation in roughness along the x-sections used within 1D hydraulic modelling.

Roughness can be modelled by changing Strickler coefficient for the various cross section along the length of the channel depending on how the channel and floodplain domains are set, setting different Strickler values for the channel and floodplains within the cross sections used. Values for Strickler coefficient can be easily available from literature, including values used in previous hydrodynamic studies on the Lower Var. We can model roughness in a model also by changing the Manning's value  $n$  to test the influence.

## 2.5.1 Results

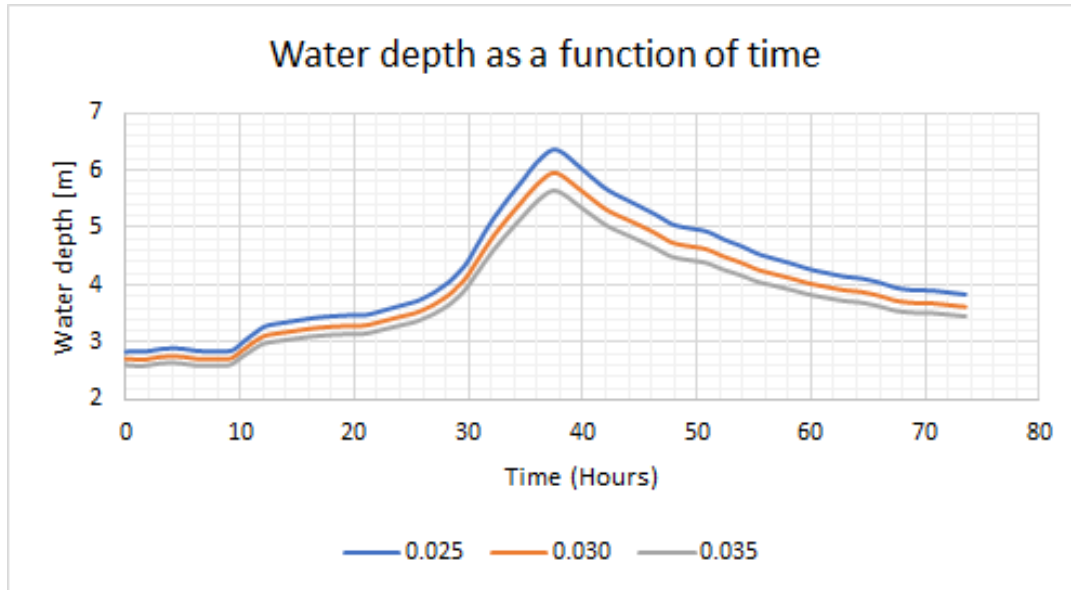


Figure 22: Water level as a function of time at different roughness coefficient

As can be seen from the graph presented above, water depth has varied with time and with the change in roughness. Higher is the roughness, lower is the level of water. Regular section in a river with no boulders and brush are assigned roughness of 0.025 and irregular rough sections are assigned the value of 0.035. The following parameters are important to look into in order to deal with uncertainties due to roughness:

- Major/Minor stream
- Top width at flood stage ( $> 100$  ft /  $< 100$  ft)
- Sections' characteristic (Regular section with no boulders or brush / Irregular and rough sections) in our case

## 2.6 Uncertainties due to weir coefficients

A weir can be understood as a low dam used to raise the level of water upstream, and to regulate flow in a river. One of the factors affecting discharge through weir is its discharge coefficient. Different types of weirs and their coefficients can be a cause of the uncertainties in this case. The discharge coefficients are normally calculated experimentally as a function of various parameters. Since it cannot be possible for each modelling case, this can also pose as a major source of uncertainty.

The effect of weir coefficients uncertainty can be explained by the used Honma formula. The higher the weir coefficient is chosen the higher the calculated discharge. In the reverse case, the water level at the

respective weir is lower. For the Weir coefficient the perfect weir coefficient is 1. Therefore, the considered areas are below one.

$$Q = \begin{cases} C_1 W (H_{us} - H_w) \sqrt{(H_{us} - H_w)} & \text{for } (H_{ds} - H_w)/H_{us} < 2/3 \\ C_2 W (H_{ds} - H_w) \sqrt{(H_{us} - H_{ds})} & \text{for } (H_{ds} - H_w)/H_{us} \geq 2/3 \end{cases}$$

Equation 11: Honma formula

Where,

Q is the discharge through structure,

W is the width,

C1 is the first weir coefficient,

C2 = (3/2)<sup>1/3</sup> C1 is the second weir coefficient,

g is the acceleration due to gravity,







H<sub>us</sub> is the upstream water level,

H<sub>ds</sub> is the downstream water level,

H<sub>w</sub> is the weir level

The uncertainties due to weir coefficients can be modelled by changing type of the weir or coefficient. The range of the values of the coefficients can be found in the table below. Since the default values from Mike11 for the Honma Formula are within the range of the Poleni Formula, the following table can be used as a guide. Here, u becomes c. For VAR the first two crest forms are assumed for possible Weir coefficients.

Table 4: Various crest types with their corresponding coefficients

crest form	μ
 broad; sharp edges	0.49-0.51
 broad; round edges	0.50-0.55
 round overfall	0.70
 sharp-edged	0.64
 rounded	0.75
 roof-shaped	0.79

Mike 11 offers several possibilities to include a weir in the model. Firstly, the broad crested type method was used. This was run through in the basic system. Here the width is given and a range for the crest level. Then the  $Q/H$  relation is calculated. The system works with a defined weir coefficient. Mike 11 also has other applications, especially three types based on formulas. In particular, the Honma formula was referred to. The width and crest level were taken from the broad crested type and only the default value of 0.49 for the Weir coefficient remained unchanged. Mike 11 displayed the error message “no monotonically increasing”. The Honma function, taken from the reference manual, was plotted into RStudio where there was no indication of the error, the function behaved monotonically and displayed the typical Weir graph. Therefore, other sources of problems were checked. For example, the elevation level of the cross section in the basic system and input parameters such as discharge were changed. However, to illustrate the theoretical uncertainties of the system, the calculated values from the broad crested type and corresponding values from the Honma formula were plotted and run through for different as coefficients.

## 2.6.1 Results

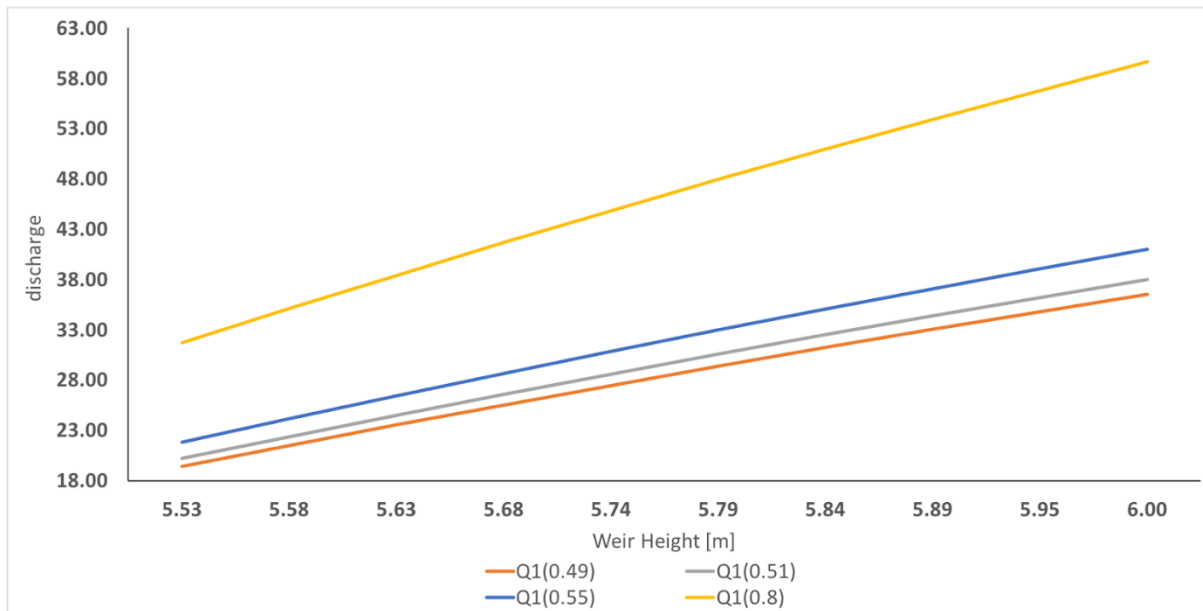


Figure 23: Discharge corresponding to various discharge coefficients

To account for the uncertainties due to weir coefficients accurately, following measures can be adopted:

- The type of weir which resembles the real structure the most should be selected in the modelling platform.
- The values of the coefficients should be chosen within the variable width and should not be based on marginal values.

## 2.7 Uncertainties due to theoretical basis

The uncertainties due to theoretical basis in 1D hydraulic modelling are based on the properties of the chosen model, such as:

- Formulas (physically based and empirical)
- St. Venant simplifications
- Numerical approximation methods

Major focus is cast on wave model approximations to demonstrate the uncertainty based on model structure looking at effects of the followings on the downstream water level:

- Fully dynamic wave
- Diffusive wave
- Kinematic wave

$$\frac{1}{A} \frac{\partial Q}{\partial t} + \frac{1}{A} \frac{\partial}{\partial x} \left( \frac{Q^2}{A} \right) + g \frac{\partial y}{\partial x} - g(S_o - S_f) = 0$$

Local  
acceleration  
term

Convective  
acceleration  
term

Pressure  
force  
term

Gravity  
force  
term

Friction  
force  
term

$$\frac{\partial V}{\partial t} + V \frac{\partial V}{\partial x} + g \frac{\partial y}{\partial x} - g(S_o - S_f) = 0$$

Kinematic Wave

Diffusion Wave

Dynamic Wave

Figure 24: Wave equations

Kinematic wave, diffusive wave and dynamic wave are the assumptions based in the equation presented above. Diffusive and kinematic wave are the simplification of the dynamic wave equation that assumes the acceleration and inertial terms are negligible for the diffusion equation.

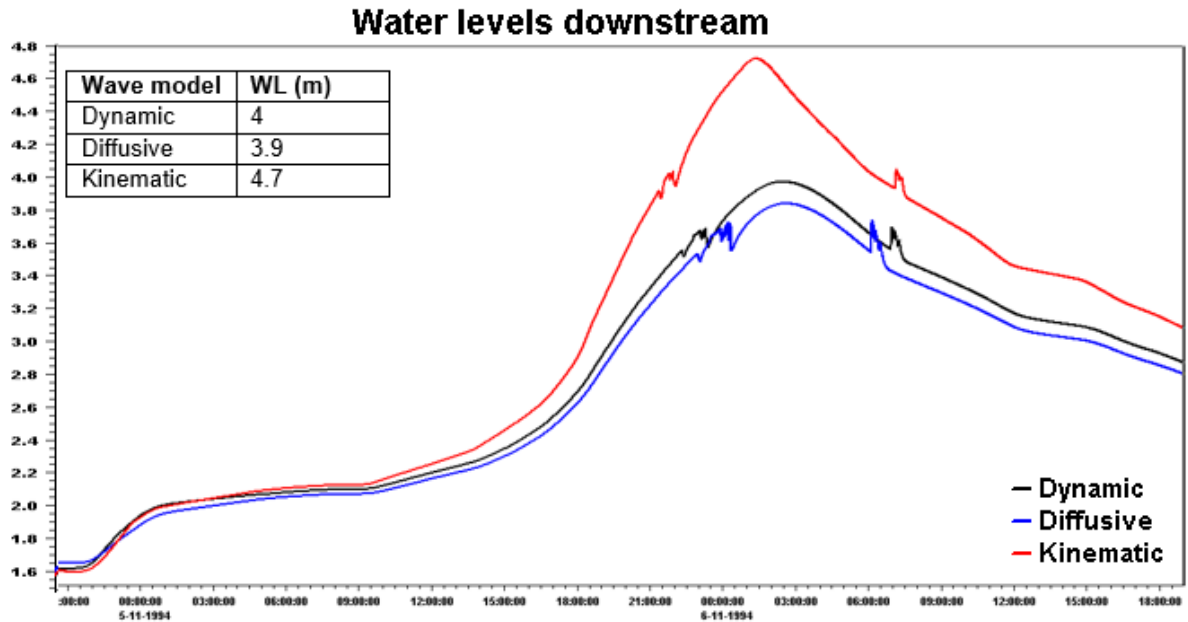


Figure 25: Downstream water level resulting from different wave models

From the graph above, it can be observed that the dynamic wave equations seems to be more reliable to use because it fully embodies the model structure (St Venant equation) whereas both the kinematic and diffusive wave models are just simplifications of the St Venant equations. The reason why we have high and low water levels using these model structures due to these assumptions in their equations.

To conclude, one can suggest based on the graph above that the fully dynamic wave models are better at depicting hydraulic flood routing than both the diffusive and kinematic wave models

## 2.8 Uncertainties due to temporal simulation time

Temporal simulation is an important consideration and source of uncertainty in 1D hydraulic modelling due to the very nature of modelling a dynamic fluvial landscape such as the Var. The Var is highly variable both seasonally in terms of discharge and sediment input into the Lower Var as well as more long-term on a decadal or multi-decadal basis.

For 1D modelling, the period being modelled should be considered: are we modelling in the Winter, the Summer, or across the whole year? Or are we trying to model or calibrate our model on a historic event to simulate a future event? Consideration for the time period being modelled, determined by the input hydrograph/upper boundary conditions, should be given in relation to several other model parameters including the channel geometry, roughness, riverbed and lower boundary condition – sea-level to name a few. All these parameters will vary due to the dynamic nature of the system. For example, if modelling the 1994 flood event to check model performance then the channel geometry should be relevant and



representative of the channel geometry during or just prior to the 1994 flood event – however, there is a large amount of uncertainty associated with this. Do we have access to reliable x-sections from 1994, are the sufficiently detailed or even accurate? Are we sure of where sediment bars were located and their extent during the flood event? – All these factors are sources of uncertainty.

Similarly, if we wanted to model predictive scenarios, how can we be sure that the flood levels determined by the 1D model are actually representative when we cannot be sure of how the channel geometry will be, or how the roughness of the river bed will be. As we saw on field trip, the removal or lowering of some of the Weirs – this action will likely affect channel morphology in situ and downstream due to changes in sediment transport and deposition.

## **2.9 Uncertainties due to flood dynamic effects**

During flood events, channel morphology and processes are subjected to changes such as collapsing of banks, collapsing of weirs, sediment transport, debris(cars, buses, fences, bricks etc.) entering the channel during extreme flood events, debris(logs, trees etc.) carried from upstream during flood events.

These changes create uncertainty in flood attenuation in blocked structures and uncertainty in flood waves due to collapsing of banks, weirs and other structures.

In order to model this uncertainty, HEC-RAS sediment transport module can be used. For this, computational simulation from one simulation can be embedded into another with updates in the geometry. Apart from this method, 2D analysis can also be approached. For breach growth, coupled 1D-2D models can be used (Mike 11-Mike21 or SOBEK 1D-SOBEK - 2D). Floating debris parameters can be used to model GeoHEC-RAS 2D can be used. It is comparatively difficult to capture and quantify this uncertainty in 1D modelling.

## **2.10 Uncertainties due to floodplain**

To determine the flood extent in a river, the use of DTM is extremely important. Therefore, quality of DTM used in hydraulic analysis is one of the major sources of uncertainty. A study by Yan et al. presented that the estimates of flood inundation uncertainty is affected by the accuracy of DTM. The quality of DTM has noticeable effect on computed flood water levels. According to Kiczko and Mirosław-Swiątek (2018), the standard deviation of calculated water level was almost the same as deviation of DTM elevations. In addition, the quality of DTM affects modelling accuracy and the correctness of the decisions related to river valley management. This effect on parameters such as flooding water level contribute to the deviation of results from real values.

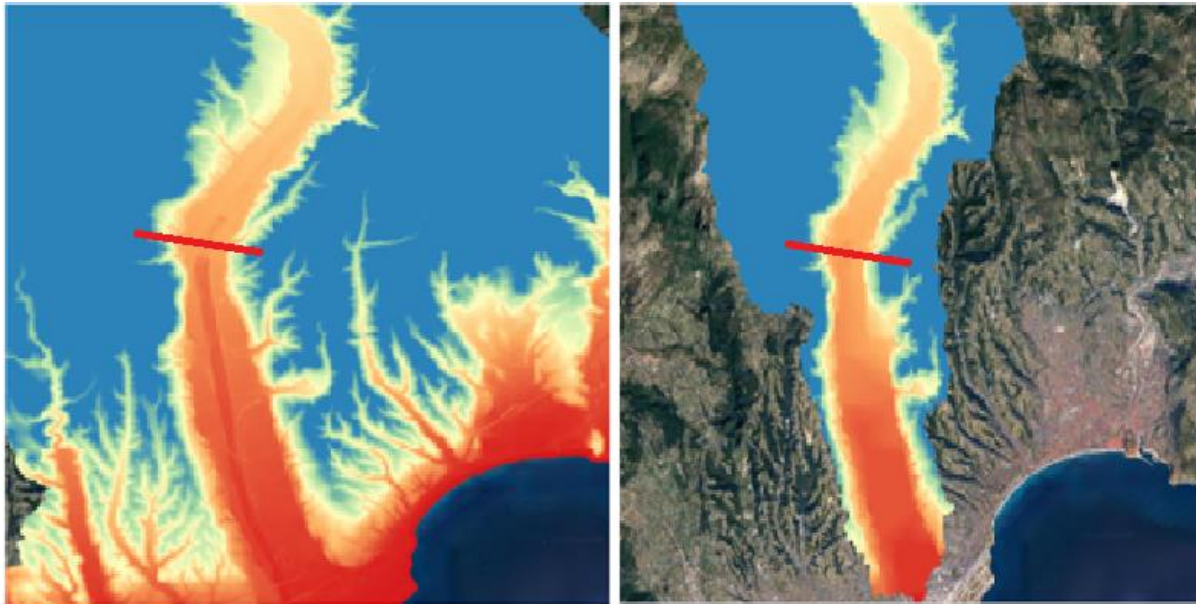


Figure 26: Figures depicting the clarity of the DEMs.

Inaccuracy of DTM is especially sensitive to 1D modelling since the cross sections are derived from the DTM. In the figure above, the left graphic shows the DEM of 5 m resolution whereas the right one shows SEM of 75 m resolution. It is seen clearly how accurately flood plain extent can be determined using 5 m resolution compared to 75 m resolution. When a section is cut from the river path, we obtain the following representation of geometry.

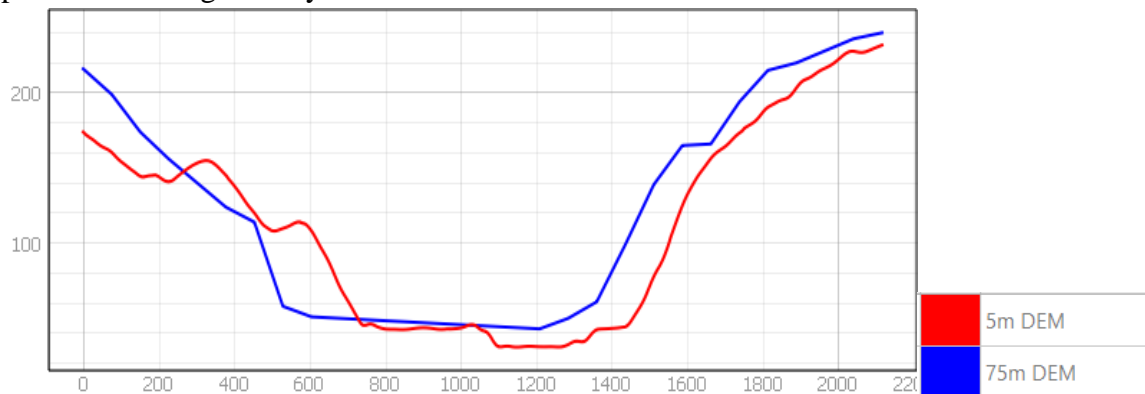


Figure 27: Cross sections of a section in a river corresponding to 5 m DEM and 75 m DEM

As per the figure it is apparent that the result for flood water level provided by 5 m DEM will be less than the result provided by 75 m DEM, which can have a significant effect in the accuracy of analysis and decision making.

## 2.11 Uncertainties due to measurement data

The major sources of data for the 1D hydraulic analysis of the Lower Var catchment include the websites like Meteo France, Vigicrue, and the archived data in the WaterEurope webpage. Since, we do not know



the process followed to extract and process this data, it is rather tough to understand and quantify the uncertainty caused by it.

## Conclusion

In this report, various factors that can develop uncertainties in a 1D hydraulic modelling were tested. The parameters that were suitable to model in Mike 11 were used to model and analyse the results, whereas the ones that could not be modelled were analysed theoretically.

## References

- Abily, M., Delestre, O., Amosse, L., Bertrand, N., Richet, Y., Duluc, C-M., Gourbesville, P., Navaro, P. (2015) Uncertainty related to high resolution topographic data use for flood event modeling over urban areas: toward a sensitivity analysis approach. *ESIAM: Proceedings and surveys*, 48, 385-399.
- Acrement, G.J. and Schneider, V.R. Guide for selecting Manning's roughness coefficients for natural channels and flood plains. Water-supply paper, U.S. Geological Survey. (1989).
- Bagat, N. (2017) Flood Frequency Analysis using Gumbel's Distribution Method: a case study of Lower Mahi Basin, India. *Journal of Water Resources and Ocean Science*, 6 (4), 51-54.
- Bozzi, S., Passoni, G., Bernardara, P., Goutal, N and Arnaud, A. (2015) Roughness and discharge uncertainty in 1D water level calculations. *Environmental Modeling & Assessment*, 20, 343-353
- Bustica, A.M., Man, T.E., Cretu, G., Badaluta, M.C. (2010) Simulation of flooding in basin of the Var river using MIKE SHE programme. *Transactions on Hydrotechnics*, 55 (69), 73-80.
- Butler, D. and Davies, J. "Urban Drainage", Chapter 7. System component and design, Taylor & Francis, 2011.
- Carleton.edu. (2018). What is measurement and uncertainty. Available: <https://serc.carleton.edu/sp/library/uncertainty/what.html>. Last accessed 27th Feb 2020.
- Chanson, H. (2004). Unsteady open channel flows: 2. Applications
- Dimitriadis, P., Tegos, A., Oikonomou, A., Pagana, V., Koukouvinos, A., Mamassis, N., ... & Efstratiadis, A. (2016). Comparative evaluation of 1D and quasi-2D hydraulic models based on benchmark and real-world applications for uncertainty assessment in flood mapping. *Journal of Hydrology*, 534, 478-492.
- Faures, J.M., Goodrich, D.C., Woolhiser, D.A., Sorooshian, S. (1995) Impact of small-scale spatial rainfall variability on runoff modeling. *Journal of Hydrology*, 173(1-4), 309-326.
- Florian Pappenberger ,Hamish Harvey ,Keith Beven ,Jim Hall , Ian Meadowcroft. Decision tree for choosing an uncertainty analysis methodology: a wiki experiment. First published:08 September 2006, <https://doi.org/10.1002/hyp.6541>
- Haan, C.T. "Statistical Methods in Hydrology." Iowa State University Press, Ames, Iowa. Haefner, Journal of Water, 1997.

Kiczko, A and Mirosław-Swiatek, D. (2018). Impact of Uncertainty of Floodplain Digital Terrain Model on 1D Hydrodynamic Flow Calculation. *Water*.

Miller, J. E. (1984). Basic concepts of kinematic-wave models (No. 1302). US Geological Survey

Koutsoyiannis, D. “On the appropriateness of the gumbel distribution in modelling extreme rainfall.” *Proceedings of the ESF LESC Exploratory Workshop, Bologna, Italy, October 24-25 2003*.

Mukolwe, M.M, Di Baldassarre, G., Werner, M., Solomatin, D.P. (2014) Flood modelling: parameterisation and inflow uncertainty. *Water Management*, 167, 51-60

National Research Council, 2012. Sea-Level Rise for the Coasts of California, Oregon, and Washington: Past, Present, and Future. Washington, DC: The National Academies Press. <https://doi.org/10.17226/13389>.

Neal, J.C., Bates, P.D., Fewtrell, T.J., Hunter, N.M., Wilson, M.D., Horritt, M.S. (2009) Distributed whole city water level measurements from the Carlisle 2005 urban flood event and comparison with hydraulic model simulations. *Journal of Hydrology*, 368(1-4), 42-55

Newcastle University (n.d.) Water-Europe\_RainfallGenerator\_Final.XLSX. Available: <https://sites.google.com/a/aquacloud.net/20we/hydrological-modelling/lesson-2-10---rainfall-generator> Accessed: 19/02/2020

Overeem, A., Buishand, A., Holleman, I (2008) Rainfall depth-duration-frequency curves and their uncertainties. *Journal of Hydrology*, 348, 112-134.

Twala, C.M., van Rensburg, L.D., Schall, R., Mosia, S.M., Dlamini, P. (2017) Precipitation intensity-duration-frequency curves and their uncertainties for Ghaap plateau. *Climate Risk Management*, 16, 1-9.

Van de Beek, C.Z., Leijnse, H., Stricker, J.N.M., Uijlenhoet, R., Russchenberg, H.W.J. (2010) Performance of high-resolution X-band for rainfall measurement in The Netherlands. *Hydrology and Earth Systems Science*, 14(2), 205-221.

Vatanchi, S.M., and Maghrebi, M.F. (2019) Uncertainty in rating curves due to Manning roughness coefficient. *Water Resources Management*, 33, 5153-5167

Viglione, A., and Blöschl, G. (2009) On the role of storm duration in the mapping of rainfall to flood return periods. *Hydrology and Earth System Sciences Discussions*, 5, 3419-3447.

Visionlearning. (2008). Uncertainty, Error and Confidence. Available: <https://www.visionlearning.com/en/library/Process-of-Science/49/Uncertainty-Error-and-Confidence/157>. Last accessed 27th Feb 2020.

Wohl, E.E. (1998) Uncertainty in flood estimates associated with roughness coefficient. Journal of Hydraulic Engineering, 124(2), 219-223

Yan, K.; Di Baldassarre, G.; Solomatine, D.P. Exploring the potential of SRTM topographic data for flood inundation modelling under uncertainty. J. Hydroinform. 2013, 15, 849–861.